Physics – Uspekhi **55** (5) 465 – 488 (2012)

REVIEWS OF TOPICAL PROBLEMS

PACS numbers: **47.65. – d**, 66.10.Ed, **82.45. – h**

Electrohydrodynamics

A I Zhakin

DOI: 10.3367/UFNe.0182.201205b.0495

Contents

1. Introduction **465**

2. System of electrohydrodynamic equations and boundary conditions **466**

2.1 Electrohydrodynamic (EHD) approximation. Basic system of EHD equations; 2.2 Thermodynamics of liquid dielectrics. Internal energy balance; 2.3 Contact processes. Problem of boundary conditions

3. Free surface in an electric field **469**

3.1 Charge balance on the free surface. Surface conductivity; 3.2 Ionic structure of the free surface; 3.3 Surface tension in an electric field

4. Main types of EHD models **472**

4.1 Ohmic conduction model; 4.2 Multiion dissociation–injection models; 4.3 EHD equations in alternating external fields

5. Dimensionless criteria. EHD approximations **475**

6. Nonstationary and transient processes **476**

6.1 Nonlinear ion waves; 6.2 Alternation of conduction modes; 6.3 Acoustic waves

7. EHD instability and development of EHD flows for symmetric electrodes **479**

7.1 EHD instability in a flat capacitor; 7.2 EHD instability in a cylindrical capacitor

8. Asymmetric electrode systems **482**

8.1 Peculiarities of EHD flows for asymmetric electrodes; 8.2 EHD flows in a plane–curved electrode system; 8.3 Numerical analysis of EHD flows; 8.4 EHD heat exchange

9. Conclusion **486**

References **487**

Abstract. The basic principles of electrohydrodynamics (EHD) are reviewed, including governing equations and boundary conditions, the applicability of EHD models, and averaged equations in alternating external fields. Dimensionless criteria for key aspects of electric and EHD processes are given. Experimental data on and theoretical treatments of basic EHD phenomena, such as transient processes, sound waves in an electric field, EHD instabilities, EHD flows, and EHD heat exchange, are discussed.

1. Introduction

Electrohydrodynamics (EHD) constitutes an interdisciplinary science encompassing such tightly entangled branches as hydrodynamics, electrostatics, electrochemistry, and thermophysics. The object of EHD research is weakly-conducting fluids (liquid dielectrics, hydrocarbon oils and fuels, etc.) having as low a conductivity as $\sigma \leqslant 10^{-7} - 10^{-12}\ \Omega^{-1}\ \mathrm{cm}^{-1}$. Nevertheless, it is the electric conduction that underlies a number of remarkable phenomena, such as EHD flows and the stabilization and destabilization of jets and droplets.

Although EHD flows have been known since Faraday's times, the intensive development of EHD began only in the 1960s, both in the USA (Melcher's group [1, 2]) and in Europe (French, Spanish [3–6], and other [7, 8] research centers). In the USSR, EHD developments were based at the Institute of Mechanics, Moscow State University [9], and Kharkov State University [10]; they were focused on theoretical aspects of EHD from the standpoint of mechanics. Extensive EHD studies using methods of applied physics were conducted at the Institute of Applied Physics, Moldavian Academy of Sciences [11], and by G A Ostroumov's scientific school at Leningrad State University [12]. At present, these investigations are being successfully continued in the Research and Educational Center, Saint Petersburg State University [13]. Certain EHD issues concerning the stability of nonuniformly heated low-conducting fluids and retention of bubbles and droplets by an electric field were investigated at Perm State University [14–16]. Specialists interested in breakdown phenomena have done a large amount of work on electrophysical processes induced in dielectric fluids by high-voltage fields [17–21]. Results of EHD research for the period from 1960 to 2000 are summarized in several books [22, 23] and reviews [24–26].

Electrostatic technologies are currently well known and found wide application in such areas as fabrication of thin filaments and capillaries [27, 28], electrostatic painting [1] and dust catching [29], and inkjet printing [30]. Attempts to create

A I Zhakin Kursk State Technical University,
ul. 50-let Oktyabrya 94, 305040 Kursk, Russian Federation
Tel. +7 (4712) 56 05 90. Fax +7 (4712) 56 18 85
E-mail: zhakin@mail.ru

Received 16 June 2011, revised 4 July 2011
Uspekhi Fizicheskikh Nauk **182** (5) 495 – 520 (2012)
DOI: 10.3367/UFNr.0182.201205b.0495
Translated by Yu V Morozov; edited by A Radzig

EHD pumps [11, 13, 22] and EHD thermostatic technologies [8, 11] have good prospects of success.

Nevertheless, many electrophysical and elelectrohydrodynamic effects remain unanticipated and unexplained to this day. For example, the free surface in a cylindrical capacitor is attracted to the central electrode in the low-field region, and repulsed from it in the high-field region [31]. Persistent dimple-like deformations are formed on an initially flat charged surface [32] that, therefore, deflects in the opposite direction to the surface force action. Disperse particles near an electrode imbedded in a liquid dielectric execute peculiar oscillatory motion, being attracted to and repulsed from it [12]. An unexpected observation is the clustering of charged disperse particles (glass spheres) in low-temperature low-pressure plasma [33]. The physical mechanism of such clustering remains to be elucidated and an analysis of cluster stability is needed, which might be analogous to the known Earnshaw theorem on the instability of equilibrium state of a system of charges [34]. In biology, the role of an electric discharge in the initiation of egg division for cloning remains enigmatic [35]. The standard explanation that a microdischarge is an equivalent to the process of egg penetration by a sperm is unconvincing, because the physicochemical processes underlying the two phenomena are different. One cannot help mentioning the phenomenon of ball lightning that is always in the focus of attention [36]. This list can be continued, but the above examples seem to be enough to illustrate the poor knowledge of electrophysical and electrohydrodynamic effects and the necessity of their further investigation. It should be noted that the unpredictability of many EHD effects is due to the complicated nonlinear character of physicochemical processes, making it difficult to study them.

The present review is designed to draw up a picture of development of EHD effects in liquid dielectrics within a wide range of electric field strengths based on the classical concepts of physicochemical processes in a bulk and at the liquid–electrode or liquid–gas interface. The review extends the cycle of previous publications [24, 25] concerning electrophysical and electrohydrodynamic properties of liquid dielectrics and the development of relevant applications.

2. System of electrohydrodynamic equations and boundary conditions

2.1 Electrohydrodynamic (EHD) approximation. Basic system of EHD equations

In the EHD approximation, radiation emitted by moving charges is neglected and the electric field energy is assumed to be much higher than the magnetic field energy. For practical purposes, the conditions of nonrelativistic approximation $V \ll c$ and medium density $\lambda \ll L$ (V is the velocity, λ is the mean free path, L is the characteristic overall size) should be supplemented by the EHD approximation conveniently written down in the form of inequalities

$$\frac{\varepsilon\omega L}{c} \ll 1\,, \qquad \frac{\sigma L}{\varepsilon c} \ll 1\,, \tag{1}$$

where ε is the relative permittivity, σ is the medium conductivity, ω is the external electric field frequency, and c is the speed of light. The first inequality is referred to as the electrostatic approximation condition, while the second one defines the smallness of the magnetic energy compared with the electric one (i.e., currents in the medium are so weak that the magnetic field they induce may be disregarded).

The system of EHD equations can be written out in different forms. The application of the apparatus of irreversible thermodynamics [37, 38] leads to a rather cumbersome set of equations taking account of small additional terms describing thermo- and barodiffusion, the electrocaloric effect, etc. In the case of low-conducting media, such as liquid dielectrics and weakly ionized dense gases, the basic set of equations is usually written in the (SI system) form [1–12]

$$\rho\left(\frac{\partial V_i}{\partial t} + V_k\,\frac{\partial V_i}{\partial x_k}\right) = \frac{\partial}{\partial x_k}\,(p_{ik} + T_{ik}) + \rho f_i\,, \quad \frac{\partial\rho}{\partial t} + \frac{\partial\rho V_i}{\partial x_i} = 0, \tag{2}$$

$$\frac{\partial\varepsilon\varepsilon_0 E_i}{\partial x_i} = q\,, \qquad E_i = -\frac{\partial\varphi}{\partial x_i}\,, \qquad \frac{\partial q}{\partial t} + \frac{\partial j_i}{\partial x_i} = 0\,. \tag{3}$$

Here, ρ is the medium mass density, V_i are the velocity components, f_i is the mass density of external forces, p_{ik} and T_{ik} are the components of mechanical and Maxwell stress tensors, E_i and φ are the electric field strength and potential, q is the volume charge density, j_i denotes components of the total electric current density $\mathbf{j}$, ε_0 is the electric constant, and i, $k = 1, 2, 3$.

Equations (2) are mechanical ones: the first equation defines the balance of momenta at an arbitrary point of the medium, while the second is the continuity equation. Relations (3) are electrostatic equations.

The system of equations (2), (3) is closing with the help of usual relations

$$p_{ik} = -p\delta_{ik} + \tau_{ik}\,, \qquad T_{ik} = -\left(\frac{1}{2}\,\varepsilon\varepsilon_0 E^2 - p_{\rm str}\right)\delta_{ik} + \varepsilon\varepsilon_0 E_i E_k\,, \tag{4}$$

$$p_{\rm str} = \frac{\varepsilon_0}{2}\,\rho\,\frac{\partial\varepsilon}{\partial\rho}\,E^2\,,$$

$$\mathbf{j} = \mathbf{j}^* + q\mathbf{V}\,, \tag{5}$$

where p is the mechanic pressure, τ_{ik} denotes components of a viscous stress tensor, $p_{\rm str}$ is the striction pressure, $\mathbf{j}^*$ is the migration current, and $q\mathbf{V}$ is the convective current.

2.2 Thermodynamics of liquid dielectrics. Internal energy balance

In the case of a nonuniformly heated fluid, the equation for internal energy balance is needed. It is recognized, when defining the thermodynamic system as a medium + field system, that the energy balance of the small system element in terms of specific quantities is written out in the form [38, 39]

$$\rho\,\mathrm{d}u' = \rho T\,\mathrm{d}s - \rho p'\,\mathrm{d}\left(\frac{1}{\rho}\right) + \mathbf{E}\,\mathrm{d}\mathbf{D}\,. \tag{6}$$

Here, $\mathbf{D}$ is the electric induction vector, T is the medium temperature, u' and s are the internal energy and entropy per unit mass of the thermodynamic system, p' is the sought after parameter having the dimension of pressure [see formulas (8) and (10)].

In a multicomponent medium, relation (6) is conveniently represented in the form

$$\rho\,\mathrm{d}u = \rho T\,\mathrm{d}s - \rho\tilde{p}\,\mathrm{d}\left(\frac{1}{\rho}\right) + \mathbf{E}\,\mathrm{d}\mathbf{P} + \rho\sum_{i=1}^{\kappa}\mu_i c_i\,\mathrm{d}c_i\,, \tag{7}$$

where $u = u' - \varepsilon_0 E^2/2\rho$, $\tilde{p} = p' + \varepsilon_0 E^2/2$, $\mathbf{P}$ is the polarization vector, μ_i is the chemical potential per unit mass of the medium, c_i is the concentration of the ith component ($c_i = \rho_i/\rho$, ρ_i is the mass density of the ith component), and κ is the number of components (index $i = \kappa$ refers to the carrier fluid).

In relation (7), by u and s are meant the specific internal energy and entropy, respectively, of the medium alone, excluding the field. The introduction of free energy density $F = F(\rho, T, \mathbf{E}, c_1, c_2, \ldots, c_{\kappa-1}) = u - \mathbf{EP}/\rho - Ts$ into formula (7) yields

$$\mathrm{d}F = -s\,\mathrm{d}T - \rho p_* \,\mathrm{d}\left(\frac{1}{\rho}\right) - \frac{\mathbf{P}\,\mathrm{d}\mathbf{E}}{\rho} + \sum_{i=1}^{\kappa-1} \zeta_i c_i \,\mathrm{d}c_i\,, \tag{8}$$

where $\zeta_i = \mu_i - \mu_\kappa$, and $p_* = \tilde{p} + \mathbf{EP}$.

Integration of Eqn (8) leads to $F = F_0 + F_E$, $u = u_0 + u_E$, $p_* = p + p_E$, $s = s_0 + s_E$, and $\zeta_i = \zeta_{0i} + \zeta_{Ei}$, where the terms u_0, s_0, and ζ_{0i} are field-independent. Dielectric constant in liquids normally depends on density and temperature alone; it is described, for example, by the Lorentz–Lorenz formula [34]

$$\frac{\varepsilon - 1}{\varepsilon + 2} = \frac{4\pi}{3m}\,\beta_0 \rho + \frac{4\pi}{3}\sum_i \beta_i n_i\,, \tag{9}$$

where β_0 and m are the polarizability and mass of the carrier fluid molecules, and β_i is the ion polarizability of the ith component. In this case, one obtains

$$\begin{aligned} &F_E = -\frac{\mathbf{EP}}{2\rho}\,, \qquad u_E = \frac{\mathbf{EP}}{2} + Ts_E\,, \qquad s_E = \frac{\varepsilon_0}{2}\,\frac{\partial \varepsilon}{\partial T}\,E^2\,, \\ &\zeta_{Ei} = -\frac{\partial \varepsilon}{\partial c_i}\,\frac{E^2}{2\rho}\,, \qquad p_E = p_{\mathrm{str}} + \frac{\mathbf{EP}}{2}\,. \end{aligned} \tag{10}$$

The internal energy balance can be found using the entropy balance equation. To this effect, the energy balance equation for the whole thermodynamic system (medium + field) is postulated. The system being closed, the energy balance equation must have a divergent form; based on physical reasoning, it can be written out in the form [38]

$$\begin{aligned} \frac{\partial}{\partial t}\left[\rho\left(\frac{V^2}{2} + u\right) + \frac{\varepsilon_0 E^2}{2}\right] = -\mathrm{div}\left[\rho\left(\frac{V^2}{2} + u\right)\mathbf{V}\right. \\ \left. + \mathbf{q} + \mathbf{S} + \sum_{i=1}^{\kappa} u_i \mathbf{I}_i - \mathbf{e}_i p_{ij} V_j + p_E \mathbf{V}\right]. \end{aligned} \tag{11}$$

Here, $\mathbf{q}$, $\mathbf{S} = \mathbf{E} \times \mathbf{H}$ are the heat flux density and electromagnetic energy density vectors, u_i and $\mathbf{I}_i$ are internal energy mass density and mass flux density of the ith component, $\mathbf{e}_i$ denotes Cartesian unit vectors, and p_E is the polarization pressure. Further on, using the kinetic energy balance equation

$$\frac{\partial}{\partial t}\left(\rho\,\frac{V^2}{2}\right) = -\mathrm{div}\left[\left(\rho\,\frac{V^2}{2}\right)\mathbf{V} + \mathbf{e}_i p_{ij} V_j\right] - p_{ij}\,\frac{\partial V_j}{\partial x_i} + V_i\,\frac{\partial T_{ij}}{\partial x_j}$$

and the identity

$$\frac{\partial}{\partial t}\left(\frac{\varepsilon_0 E^2}{2}\right) = -\mathrm{div}\,\mathbf{S} - \mathbf{E}\,\frac{\partial \mathbf{P}}{\partial t} - \mathbf{jE}\,,$$

we obtain from equation (11) the internal energy balance equation that is transformed, after simple rearrangements, to the standard form [37]

$$\begin{aligned} &\rho\left(\frac{\mathrm{d}u_0}{\mathrm{d}t} + \frac{\mathrm{d}(Ts_E)}{\mathrm{d}t}\right) = -\mathrm{div}\left(\mathbf{q} + \sum_{i=1}^{\kappa} u_i \mathbf{I}_i\right) - p\,\mathrm{div}\,\mathbf{V} + \dot{\xi}_T + \dot{\xi}_P\,, \\ &\dot{\xi}_T = \mathbf{j}^*\mathbf{E} + \tau_{ij}\,\frac{\partial V_j}{\partial x_i}\,, \qquad \dot{\xi}_P = p_{\mathrm{str}}\,\mathrm{div}\,\mathbf{V} + \frac{\varepsilon_0 E^2}{2}\,\frac{\mathrm{d}\varepsilon}{\mathrm{d}t}\,. \end{aligned} \tag{12}$$

Here, $\mathrm{d}/\mathrm{d}t = \partial/\partial t + \mathbf{V}\nabla$ is the total derivative, $\dot{\xi}_T$ is the Joule and viscous heat release, and $\dot{\xi}_P$ is the heat release due to medium repolarization. It should be noted that frequency limitation (1) holds up to 10^9 Hz; however, the assumption of instantaneous relaxation of polarization is invalid in the frequency range of 10^3 Hz. This results in medium heating due to dipole rotation. Then, dielectric loss is written as

$$\dot{\xi}_P = 0.5\omega\varepsilon\varepsilon_0 E^2 \tan\varphi\,, \tag{13}$$

where $\tan\varphi$ is the tangent of the dielectric loss angle [17, 18].

Combining Eqns (7) and (12) leads to the entropy balance equation coinciding with the one in monograph [37] that provides a basis for the derivation of closing relations for thermodynamic fluxes $\mathbf{q}$, $\mathbf{I}_i$, p_{ij} by standard methods of irreversible thermodynamics. Finally, equation (12), on the assumption of $u_0 = u_0(T)$, $\mathbf{q} = -\lambda\nabla T$, becomes the form of a heat conduction equation taking into account the dielectrocaloric effect [the term $\rho\,\mathrm{d}(Ts_E)/\mathrm{d}t$] and heat release due to medium compressibility and various physicochemical processes.

For multicomponent media, such as liquid dielectrics, one has $u_0 = \sum_{i=1}^{\kappa} u_{i0} c_i$, where u_{0i} is the internal energy of the ith component. Further on, using the ion component balance equation [37, 40]

$$\rho\,\frac{\mathrm{d}c_i}{\mathrm{d}t} = -\mathrm{div}\,\mathbf{i}_i^* + \dot{\xi}_i\,, \tag{14}$$

where $\mathbf{i}_i^*$ stands for partial densities of particle fluxes (see Section 2.3), and taking account of $c_\kappa \sim 1$, $c_i \ll 1$, $i = 1, \ldots, \kappa - 1$ and the thermodynamic relation

$$\frac{\mathrm{d}u_{\kappa 0}}{\mathrm{d}t} = \frac{\partial u_{\kappa 0}}{\partial T}\,\frac{\mathrm{d}T}{\mathrm{d}t} + \frac{\partial u_{\kappa 0}}{\partial \rho}\,\frac{\mathrm{d}\rho}{\mathrm{d}t} = c_v\,\frac{\mathrm{d}T}{\mathrm{d}t} + \left(p - T\,\frac{\partial p}{\partial T}\right)\frac{1}{\rho^2}\,\frac{\mathrm{d}\rho}{\mathrm{d}t}\,,$$

yield

$$\begin{aligned} \rho c_v\,\frac{\mathrm{d}T}{\mathrm{d}t} + \rho\,\frac{\mathrm{d}(Ts_E)}{\mathrm{d}t} = -\mathrm{div}\,\mathbf{q} - \sum_{i=1}^{\kappa} \mathbf{i}_i^* \nabla u_{i0} \\ - T\,\frac{\partial p}{\partial T}\,\mathrm{div}\,\mathbf{V} + \dot{\xi}_T + \dot{\xi}_P + \dot{\xi}_x\,, \end{aligned} \tag{15}$$

$$\dot{\xi}_x = -\sum_{i=1}^{\kappa} u_{i0}\dot{\xi}_i\,, \tag{16}$$

where $\dot{\xi}_x$ is the heat release due to chemical reactions, and c_v is the specific heat at a constant volume. In particular, for a monomolecular reaction of ion pair decomposition (see Section 3.2), one obtains

$$\dot{\xi}_x = -h_0\dot{\xi}\,, \qquad h_0 = u_{10} + u_{20} - u_{30}\,, \tag{17}$$

where h_0, $\dot{\xi}$ are the thermal effect and the decomposition rate, respectively, u_{30} is the internal energy of ion pairs, and u_{10} and u_{20} are the internal energies of monoions (reaction products).

2.3 Contact processes. Problem of boundary conditions

In order to describe electrical conduction of multicomponent media, partial densities of ith component fluxes are introduced, $\mathbf{i}_i^*$, such that $\mathbf{j}^* = \sum_i e_i \mathbf{i}_i^*$ (hereinafter, the symbol $\sum_i$ denotes summation over all ionic components). The fluxes $\mathbf{i}_i^*$ are given by the following kinetic relations

$$\mathbf{i}_i^* = -D_i \nabla n_i + (\operatorname{sign} e_i)\, b_i n_i \mathbf{E}\,, \tag{18}$$

where D_i and b_i are the coefficients of ion diffusion and mobility, respectively, and e_i and n_i are the charge and the concentration of the ith sort of ions.

The balance equations for concentrations n_i of ion components are determined by continuity equations with $\dot{\xi}_i$ sources (see, for instance, books [37, 40]):

$$\frac{\partial n_i}{\partial t} + \operatorname{div}(\mathbf{i}_i^* + n_i \mathbf{V}) = \dot{\xi}_i\,, \tag{19}$$

where $\dot{\xi}_i$ depends on chemical reactions between the charged components (see Section 4.2).

Determination of boundary conditions for equations (19) is one of the most difficult problems in electrophysics. Formulation of universal boundary conditions in EHD is impossible due to the interference of various physical and chemical processes that may occur in the high-voltage field region, depending on the properties of the electrode surface and the fluid. From the mathematical standpoint, there are two approaches, with partial currents $\mathbf{i}_i^*$ in one of them and concentrations of the injected ionic components in the other specified at the boundaries. The choice of the boundary conditions requires a thorough investigation of contact processes, which accounts for the aforementioned difficulty. Let us consider certain generally accepted models of injection processes.

2.3.1 Electron emission. Strong electric fields initiate two types of electron emission from the surface of metallic electrodes [41, 42].

Emission of the first type is related to lowering the potential barrier at the metal boundary by ΔU_E; this quantity is calculated in the following way. Let r_0 be the characteristic atomic size. The potential energy of an electron at distance $x \gg r_0$ is found taking account of the image force potential as [41] $\Pi = U_0 - \Delta U_E(x)$, where $\Delta U_E(x) = e^2/16\pi\varepsilon\varepsilon_0 x + eEx$, with x being the coordinate directed from the metal surface to the interior of the liquid. Function $\Delta U_E(x)$ passes through a minimum at $x_* = \sqrt{e/16\pi\varepsilon\varepsilon_0 E}$. Hence, $\Delta U_E = \Delta U_E(x_*) = e\sqrt{eE/4\pi\varepsilon\varepsilon_0} = \Phi_E$, and field-amplified electron injection is governed by the Schottky law

$$j = j_0(T) \exp \frac{\Phi_E}{k_B T}\,, \qquad \Phi_E = e\sqrt{\frac{eE}{4\pi\varepsilon\varepsilon_0}}\,, \tag{20}$$

where $j_0(T)$ is the thermionic current governed by the Richardson–Dushman expression

$$j_0(T) = AT^2 \exp\left(-\frac{\Phi_m}{k_B T}\right).$$

Here, $A = A_0(1 - \bar{r})$, where $\bar{r}$ is the coefficient of electron reflection from the metal–vacuum interface averaged over energies, $A_0 = 120.4\ \mathrm{A\,cm^{-2}\,K^{-2}}$, and Φ_m is the electron work function of a metal. The value of coefficient A, essentially dependent on surface characteristics (the presence of oxide films, adsorbed ions, defects, pores, etc.), lies in a range of $15-350\ \mathrm{A\,cm^{-2}\,K^{-2}}$ [41]. The metal work function varies from 2.2 to 4.5 eV, with the lowest values in alkali metals (Li — 2.5 eV, Na — 2.3 eV, K — 2.2 eV) and the highest ones in typical metals (Cu, Ag — 4.5 eV, Au — 4.9 eV, Al — 4.2 eV, Fe — 4.4 eV, W — 4.5 eV). At room temperature, $k_B T = 1/40$ eV.

Because factor $\exp(-\Phi_m/k_B T)$ takes extremely low values [on the order of $\exp(-80) \approx 10^{-35}$], the thermionic currents are practically absent at room temperature. A decrease in potential for nonpolar dielectrics ($\varepsilon = 2.2$) is only $\Phi_E \sim 0.08$ eV, even at breakdown voltages of $E = 10^7\ \mathrm{V\,m^{-1}}$.

This means that Schottky injection into a liquid dielectric plays an important role only in the case of extremely low work functions, e.g., in the presence of adsorbed layers or metallized oxide films [41]. As a matter of practice, the surfaces of metallic electrodes are almost always coated with oxide films. Oxides of the most widespread metals have rather high work functions (copper oxides — 1.8–5.15 eV, iron — 3.4–3.8 eV, titanium — 3.0–6.2 eV, zinc — 3.9–5.0 eV, Al — 3.8–4.7 eV [32]). Therefore, it can be concluded that in the absence of charged adsorbed layers the Schottky injection from the cathode to a liquid dielectric in pre-breakdown electric fields is insignificant. This inference is confirmed by the data on volt–ampere characteristics (VACs) that, as a rule, show quadratic dependence [13, 24] under conditions of fully developed electroconvection.

The second type of electron emission observed in strong fields ($E > 10^3\ \mathrm{kV\,cm^{-1}}$) covers cold electron emission from the cathode, the currents of which are described by the Fowler–Nordheim law

$$j = AE^2 \exp\left(-\frac{B}{E}\right). \tag{21}$$

In electrohydrodynamics, the cold electron emission has influence only in the case of very sharp-pointed negative electrodes regarded in applied EHD as inefficient injectors unable to maintain fairly well-developed electroconvection.

2.3.2 Ion injection. Once physically adsorbed ions are retained at the metal surface by image forces, ion injection in strong fields is feasible from both the cathode and anode [43]. Generally, the surface ions may be generated in reversible redox reactions, e.g., $\mathrm{X} + \mathrm{e}^- \leftrightarrow \mathrm{X}^-$ at the cathode. Here, X is the electron acceptor that is, as a rule, the chemically active part of a molecule (iodine and bromine atoms in hydrogen halides like iodobenzene and bromobenzene, respectively) or $\mathrm{I_2}$ molecules in nonpolar hydrocarbon dielectric solutions [44–46]. The direct and reverse reactions are characterized by rate constants k_{X1} and k_{X2}, respectively. Their calculation in the general case is an extremely difficult task due to, first, the lack of information on the real surface structure (the presence of defects, roughness, films, etc.) and, second, the necessity of taking into account effects of the double electric (diffusion) layer, the structure of which is generally unknown.

The following line of reasoning is based on general theoretical concepts and models. There are two different reaction channels. In the absence of an external field (or in weak fields), electron transitions are due to the overlap of electron orbitals [47]. Such cases are usually associated with strong chemosorption of X^- ions. In strong fields, electrons are 'pulled out' from the conduction band to form two-

dimensional electron clouds [48–51] with a surface concentration n_{se}. In this case, the rate of direct reaction $X + e^- \to X^-$ is expressed as $\dot{\xi} = \langle V_e \sigma_e \rangle n_{se} c_X$ [52], where c_X is the concentration of neutral atoms X, and V_e and σ_e are the electron capture rate and cross section (angle brackets denote averaging over electron velocities). Hence, rate constant k_{X1} has the form

$$k_{X1} = \langle V_e \sigma_e \rangle n_{se} \,. \tag{22}$$

In both cases, electrode surface concentrations n_i of the charges being injected can be specified as functions of the electric field strength at the electrode. By way of example, for reaction $X + e^- \leftrightarrow X^-$ one has [23, 53]

$$n_i = n_c(E) \equiv \frac{k_{X1} c_X}{b_i E_{loc} + k_{X2} G(E_{loc})} \,, \tag{23}$$

$$G(E_{loc}) = \frac{e E_{loc}}{k_B T} \int_{r_0}^{\infty} \frac{g(x)}{g(r_0)} \, dx \,, \qquad g(x) = \exp \frac{\Pi(x)}{k_B T} \,,$$

$$\Pi(x) = -e E_{loc} + \Pi_i(x) \,, \qquad \Pi_i(x) = -\frac{e^2}{16\pi\varepsilon\varepsilon_0 x} \,.$$

Here, b_i and r_0 are the mobility and the effective size of X^- ions, $\Pi_i(x)$ is the image force potential, E_{loc} is the local field strength on the electrode surface that may be essentially different from the mean surface field E [25]. For instance, it may be assumed in the case of rough electrodes that the electric field initiates injection processes at spikes of microinhomogeneities. In this case, it is claimed that $E_{loc} = \beta_s E$, where β_s is the field amplification factor having the order of $10-10^3$ [54].

Relation (23) actually describes two processes, namely, electronic transition to the adsorbed electron acceptor X, and the subsequent activation transition of an X^- ion from the physical adsorption zone on the electrode surface to the bulk of the liquid under the action of the external electric field. Assuming that $b_i E_{loc} \ll k_{X2} G(E_{loc})$, formula (23) yields the injection function of physically adsorbed charges on the metal surface [55]:

$$n_i = \frac{n_0}{G(E_{loc})} \,, \tag{24}$$

where $n_0 = k_{X1} c_X / k_{X2}$ is the constant concentration of the adsorbed ions.

It is worth noting that function $G(E_{loc})$ for point ions ($r_0 \to 0$) is transformed to the modified zero-order Bessel function: $G(E_{loc}) \to I_0(E_{loc})$, having exponential asymptotics analogous to Schottky injection (20) in the strong field region.

It is commonly supposed [41] that relations (20), (21), similar to (23), (24), hold true in idealized cases where the electrode surface is flat and free of defects. In real situations, even thoroughly polished electrodes have roughnesses [56] and defects that serve as adsorption centers making injection processes possible (Fig. 1). Formation of the injection centers is complicated by the presence of active components capable of electrochemical transformations. For instance, peculiar spiral EHD movements spreading out from fixed centers are known to occur in thin layers of ferromagnetic colloid stabilized by oleinic acid [57, 58] (Fig. 2). We believe the geometric centers of these structures to be sites of electrochemical injection of the charges that induce either EHD movements or autowave chemical reactions [59]. It is noteworthy that the formation of injection centers on

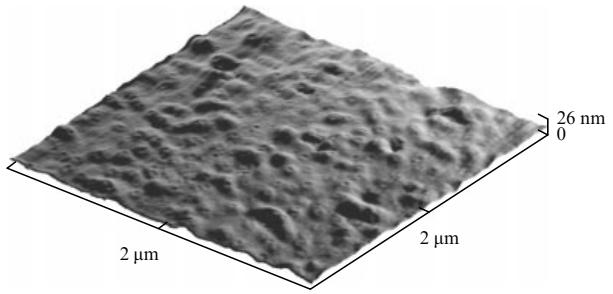

Figure 1. Atomic-force microscopy (AFM) image of a thoroughly polished copper surface (roughness size is not more than 20 nm) [56].

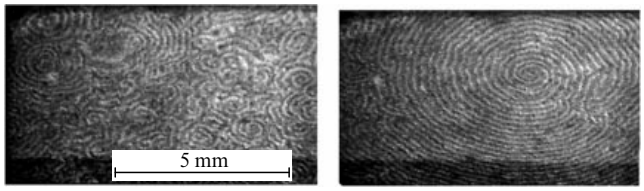

Figure 2. Pictures of pulsed EHD movements in the thin layer of a ferromagnetic fluid: the scale and shapes of spiral structures (taken from Refs [57, 58]).

electrode surfaces is typical of surface electron processes, as evidenced, for example, by the results of electron emission microscopy [41]. Also, it is worth mentioning that the impurity adsorption on the electrodes strongly depends on the electrode material, electric field strength, and current passage time. For example, the ampere–time characteristics of transformer oil solutions containing iodine in a flat capacitor suggest that conductivity in the case of copper electrodes at a mean field strength of $E = U/d = 7.3\ \mathrm{kV\,cm^{-1}}$ decreases more than tenfold for 4 hours. In the case of titanium electrodes, it does not change during the same time [60].

Although formulas (20), (21), (24) have been derived for idealized conditions, they are in satisfactory agreement with experimental evidences. In such a way, as shown in Ref. [25], the surface electron concentration n_{se} induced by a high-voltage field is proportional to the local strength squared, $n_{se} \sim E_{loc}^2$, in agreement with both quadratic VACs and EHD flow velocities. In this case, the so-called linear injection law follows from expression (24) at the low reverse reaction rate [25, 53]:

$$n_i = \eta_c E \,, \tag{25}$$

where η_c is the injection coefficient at the cathode.

There is one more, very specific, type of ion injection from ionite membranes into polar fluids. Such injection is realized when dielectric constant of the fluid is so high that ions are 'pulled out' of the membrane into the bulk of the liquid dielectric. In this case, the concentration of the ions being injected is assumed to be constant at the membrane, and the injection itself is called autonomous [3–5].

3. Free surface in an electric field

In studies of surface effects, the finite surface conductivity is normally disregarded and in addition the surface tension

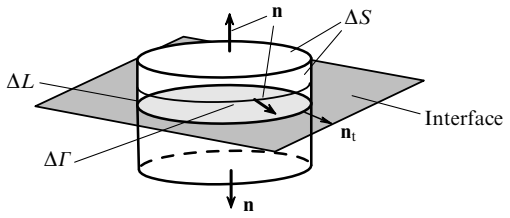

Figure 3. The choice of reference volume ΔW.

coefficient is assumed to be independent of the electric field. In what follows, we consider justification of these assumptions and discuss discrepancies in the formulation of surface charge balance on a free surface (see, for instance, Refs [1, 2, 23, 38, 61]).

3.1 Charge balance on the free surface. Surface conductivity

The balance equation for the concentration n_{si} of surface charges of the ith component is derived by a standard method [62]. First, the balance of the number of charges is written down in the integral form for a material volume ΔW encompassing a small part of the surface $\Delta\Gamma$ in the local system of coordinates (Fig. 3):

$$\frac{\mathrm{d}}{\mathrm{d}t}\int_{\Delta\Gamma} n_{si}\,\mathrm{d}S = -\int_{\Delta L}\mathbf{i}_{si}^{*}\mathbf{n}_{\mathrm{t}}\,\mathrm{d}l - \int_{\Delta S}\mathbf{i}_{i}^{*}\mathbf{n}\,\mathrm{d}S + \int_{\Delta\Gamma}\dot{\xi}_{si}\,\mathrm{d}S, \quad (26)$$

where ΔL is the contour encircling $\Delta\Gamma$, $\mathbf{n}_{\mathrm{t}}$ is the surface external normal to ΔL, ΔS is the ΔW volume boundary, $\mathbf{n}$ is the external normal to ΔS, $\mathbf{i}_{si}^{*}$ and $\mathbf{i}_{i}^{*}$ are migration surface and bulk fluxes, and $\dot{\xi}_{si}$ is the source of surface charge generation. Then, using the formula for the derivative of the material volume [63–65], namely

$$\frac{\mathrm{d}}{\mathrm{d}t}\int_{\Delta\Gamma} n_{si}\,\mathrm{d}S = \int_{\Delta\Gamma}\left(\frac{\partial n_{si}}{\partial t} + \mathrm{div}_{\mathrm{s}}\,(n_{si}\mathbf{V}_{\mathrm{t}}) - 2Hn_{si}V_{n}\right)\mathrm{d}S,$$

and the Gauss–Ostrogradsky formula

$$\int_{\Delta L}\mathbf{i}_{si}^{*}\mathbf{n}_{\mathrm{t}}\,\mathrm{d}l = \int_{\Delta\Gamma}\mathrm{div}_{\mathrm{s}}\,\mathbf{i}_{si}^{*}\,\mathrm{d}S,$$

after shrinking the volume ΔW to a point, we obtain from formula (26) the following balance equation for the surface charge concentration:

$$\frac{\partial n_{si}}{\partial t} + \mathrm{div}_{\mathrm{s}}\,(\mathbf{i}_{si}^{*} + n_{si}\mathbf{V}_{\mathrm{t}}) - 2Hn_{si}V_{\mathrm{n}} = -[i_{\mathrm{in}}^{*}] + \dot{\xi}_{si}. \quad (27)$$

Here, $\mathbf{V}_{\mathrm{t}}$ is the tangential velocity component at the surface, H is the mean surface curvature, and V_{n} and i_{in} are the normal components of vectors $\mathbf{V}$ and $\mathbf{i}_i$.

The question arises as to the determination of surface fluxes $\mathbf{i}_{si}^{*}$ and sources $\dot{\xi}_{si}$ for each ion type. In the case of ion activation motion, the surface flux is found in analogy to relation (18):

$$\mathbf{i}_{i}^{*} = -D_{si}\nabla_{\mathrm{s}}n_{si} + (\mathrm{sign}\,e_i)b_{si}n_{si}\mathbf{E}_{\mathrm{t}}, \quad (28)$$

where D_{si} and b_{si} are surface diffusion and mobility coefficients, respectively, $\mathbf{E}_{\mathrm{t}}$ is the tangential field component, and ∇_{s} is the surface gradient [63, 64].

Sources $\dot{\xi}_{si}$ can be determined by introducing surface ion pairs and dissociation–recombination interactions. However, there are important peculiarities in the determination of sources ξ_{si}, which are related to the catalytic activity of the surface [66]. Specifically, the surface may be the site of chemical and adsorption–desorption processes involving bulk matter. For this reason, determination of $\dot{\xi}_{si}$ sources is an important and, generally speaking, rather difficult task of physical chemistry.

Defining the total surface charge $q_{\mathrm{s}} = \sum_i e_i n_{si}$, current $\mathbf{j}_{\mathrm{s}}^{*} = \sum_i e_i\mathbf{i}_{si}^{*}$, and source $\dot{\xi}_{\mathrm{s}} = \sum_i e_i\dot{\xi}_{si}$ leads to the total charge balance equation derived from Eqn (27):

$$\frac{\partial q_{\mathrm{s}}}{\partial t} + \mathrm{div}_{\mathrm{s}}\,(\mathbf{j}_{\mathrm{s}}^{*} + q_{\mathrm{s}}\mathbf{V}_{\mathrm{t}}) - 2Hq_{\mathrm{s}}V_{\mathrm{n}} = -[j_{\mathrm{n}}^{*}] + \dot{\xi}_{\mathrm{s}}. \quad (29)$$

This equation was assayed without considering the terms $2Hq_{\mathrm{s}}V_{\mathrm{n}}$, $\dot{\xi}_{\mathrm{s}}$ in numerous examinations of EHD effects on charged free surfaces (see, for instance, Refs [2, 61]). Clearly, the curvature term can be disregarded in the case of flat surfaces. However, the surface curvature may be a crucial factor in the case of curved surfaces (jets, droplets, etc.), especially in studies of nonlinear effects or vibrational perturbations.

Assuming the surface diffusion coefficients of each component to be identical and taking account of formula (28), we arrive at an analog of Ohm's law for the surface current:

$$\mathbf{j}_{\mathrm{s}}^{*} = -D_{\mathrm{s}}\nabla_{\mathrm{s}}\,q_{\mathrm{s}} + \sigma_{\mathrm{s}}\mathbf{E}_{\mathrm{t}}, \qquad \sigma_{\mathrm{s}} = \sum_i e_i b_{si} n_{si}. \quad (30)$$

Generally, the surface conductivity σ_{s} is not a physical constant. The constancy of σ_{s}, similar to that of bulk conduction, is ensured on condition that surface ions are tightly bound, e.g., as a result of a dissociation–recombination reaction. If surface ions do not undergo hemosorption, i.e., they are localized in the transient layer inside the liquid (see Section 3.2), there is every reason to believe that their surface and bulk mobilities coincide: $b_{si} = b_i$.

3.2 Ionic structure of the free surface

When studying the ionic structure of the free surface, we shall assume that the liquid possesses dissociation conduction due to decomposition of $\mathrm{A^+B^-}$ ion pairs in the reversible reaction

$$\mathrm{A^+B^-} \underset{\alpha_{11}}{\overset{k_{\mathrm{d}}}{\leftrightarrows}} \mathrm{A^+} + \mathrm{B^-}, \quad (31)$$

where k_{d} is the decomposition rate constant of $\mathrm{A^+B^-}$ ion pairs, and α_{11} is the pair recombination coefficient of $\mathrm{A^+}$, $\mathrm{B^-}$ monoions. Equilibrium ion concentrations $n_1(\mathrm{A^+})$ and $n_2(\mathrm{B^-})$ are equal: $n_1 = n_2 = n_0 = \sqrt{k_{\mathrm{d}}N/\alpha_{11}}$, where N is the ion pair concentration.

Ion concentrations change near the surface: $n_i = n_i(x)$, where x is the normal coordinate having the origin on the surface and directed into the depth of the liquid. In the approximation of mean forces $\mathbf{F}_i$, concentrations $n_i(x)$ are given by the first equations of Bogoliubov's chain: $k_{\mathrm{B}}T\nabla n_i + n_i\mathbf{F}_i = 0$ $(i = 1, 2)$. Introducing mean force potentials, $\mathbf{F}_i = -\nabla\Pi_i$, leads to

$$n_i = n_0\exp\left(-\frac{\Pi_i}{k_{\mathrm{B}}T}\right), \qquad i = 1, 2. \quad (32)$$

The potential Π_i consists of two items: the potential of short-range forces $\Pi_s(x)$:

$$\Pi_s(x) = \frac{\beta}{x}\,, \qquad \beta = \frac{e^2}{16\pi\varepsilon\varepsilon_0}\,\frac{\varepsilon-1}{\varepsilon+1}\,, \tag{33}$$

and the potential $e_i\varphi$ of charge–field interaction formed by the ions and the external electric field:

$$\Pi_i = \Pi_s + e_i\varphi\,, \qquad i = 1, 2\,. \tag{34}$$

For single-charged ions, $e_1 = e$, $e_2 = -e$, which will henceforth be borne in mind. The distribution of the electric field potential is described by the Poisson equation

$$\begin{aligned} &\Delta\varphi = \frac{(n_2 - n_1)e}{\varepsilon\varepsilon_0} = \gamma\exp\left(-\frac{r_d}{x}\right)\sinh\frac{\varphi}{\varphi_0}\,,\\ &r_d = \frac{\beta}{k_B T}\,, \qquad \gamma = \frac{2en_0}{\varepsilon\varepsilon_0}\,, \qquad \varphi_0 = \frac{k_B T}{e}\,. \end{aligned} \tag{35}$$

The boundary conditions for equation (35) have the form

$$E_n = -\varepsilon\frac{d\varphi}{dx} \quad \text{at} \quad x = 0\,, \qquad \varphi < \infty \quad \text{as} \quad x \to \infty\,, \tag{36}$$

where E_n is the normal component of the external electric field strength.

For the analysis of set (35), (36), we shall introduce dimensionless variables $\Phi = \varphi/\varphi_0$, and $s = x/r_D$, where $r_D = \sqrt{\varepsilon\varepsilon_0 k_B T/2e^2 n_0}$ is the Debye radius. With the new variables, one obtains

$$\begin{aligned} &\Delta\Phi = \exp\left(-\frac{p}{s}\right)\sinh\Phi; \quad s = 0\colon \frac{d\Phi}{ds} = -\eta\,, \quad \Phi(\infty) < \infty\,,\\ &p = \frac{r_d}{r_D}\,, \qquad \eta = \frac{E_n}{E_D}\,, \qquad E_D = \frac{\varepsilon\varphi_0}{r_D}\,. \end{aligned} \tag{37}$$

At typical values of $\sigma = 10^{-12}\ \Omega^{-1}\ \text{cm}^{-1}$, $\varepsilon = 2.2$, and mobilities $b_1 \sim b_2 \sim b = 10^{-8}\ \text{m}^2\ \text{V}^{-1}\ \text{s}^{-1}$, one finds $n_0 \approx \sigma/(2eb) = 3\times10^{16}\ \text{m}^{-3}$, $r_d = 7\times10^{-9}\ \text{m}$, $r_D = 7.3\times10^{-5}\ \text{m}$, $\varphi_0 = 0.025\ \text{V}$, $E_D = 7.5\ \text{V m}^{-1}$, and parameter $p \leqslant 10^{-4}$. Due to this, factor $\exp(-p/s)$ in formulas (37) can be omitted. In this situation, one arrives at

$$\begin{aligned} &\Phi = \ln\left(2u^2 - 1 + \sqrt{(2u^2-1)^2 - 1}\,\right),\\ &u = \frac{1 + a\exp(-2s)}{1 - a\exp(-2s)}\,, \qquad a = \frac{u_0 - 1}{u_0 + 1}\,,\\ &u_0 = \cosh\frac{\Phi(0)}{2}\,, \qquad \cosh\Phi(0) = 1 + \frac{\eta^2}{2}\,. \end{aligned} \tag{38}$$

For avoidance of misunderstanding, it should be pointed out that the general solution of equation (37) at $p = 0$, presented in the classical monograph [66], contains an error.

In strong fields ($\eta \gg 1$), it follows from formulas (38) that

$$u = \frac{\eta\left[1 + \exp(-2s)\right]}{\eta - (\eta - 4)\exp(-2s)}\,, \qquad s = \frac{x}{r_D}\,. \tag{39}$$

This equation, together with the expression for Φ in Eqn (38), describes the field distribution in the flat surface case. Expression (38) shows that the thickness of an ion layer depends on the Debye radius r_D, so that $r_D \sim 73\ \mu\text{m}$ in nonpolar weakly conducting media, and $r_D \sim 10\ \mu\text{m}$ in polar ones (such as nitrobenzene, aromatic hydrocarbons, etc.). This means that the concept of ohmic conduction for charged hydrocarbon droplets and thin jets of micrometer size is invalid, since the charge is redistributed over the entire bulky liquid. Even for tap water at $\varepsilon = 81$, $\sigma = 10^{-7}\ \Omega^{-1}\ \text{cm}^{-1}$, one finds $r_D \sim 1\ \mu\text{m}$, and the surface charge concept holds true for sizes above 10 μm.

3.3 Surface tension in an electric field

Investigations into the influence of impurities on surface tension are carried out applying the thermodynamic and statistical methods [64–66]. Mathematical calculations are usually so cumbersome that a variety of assumptions are needed, which are based on a combination of thermodynamic and statistical approaches. This leads to discrepancies among the computed results (up to 30%) [67]. Therefore, such approaches are, as a rule, of a qualitative character. The results of studies on the effects of an electric field using the Gibbs isotherm method are reported below.

In the presence of impurities, a change in the surface tension coefficient α is described by the Gibbs isotherm [67–69]:

$$d\alpha = -\sum_i \Gamma_i\, d\mu_i\,, \qquad \Gamma_i = \int_{-\infty}^{\infty}\left(n_i(x) - n_i^{1,2}\right)dx\,, \tag{40}$$

where μ_i is the chemical potential per molecule (ion) of the ith component, Γ_i denotes the adsorption parameters, $n_i(x)$ are the single-particle distribution functions, and $n_i^{1,2}$ are constant phase-1 (2) bulk concentrations. The ith component exhibits positive adsorption for $\Gamma_i > 0$, and negative adsorption for $\Gamma_i < 0$, with surface tension decreasing in the former case and increasing in the latter.

Adsorption isotherm (40) is an exact relation; in other words, it is derived both from quasithermodynamics and by statistical methods [67, 68]. Therefore, the problem reduces to the calculation of $n_i(x)$. In the framework of the bi-ion dissociation conduction model (31) in the mean force approximation, these functions are defined according to formulas (34), (35). Then, the chemical potential needs to be found. For example, in the case of electrocapillary effect on a mercury surface bordering a strong electrolyte, it is assumed that [39]

$$\mu_i = \mu_{0i} + k_B T\ln n_i + e_i\varphi_i\,,$$

where φ_i is the electric field potential on the mercury surface ($i = 1$) and at the outer boundary of the double electric layer (DEL) ($i = 2$). In the calculation of surface tension in an electrolyte–gas system, it is the custom that [67]

$$\mu_i = \mu_{0i} + k_B T\ln n_i + e_i\tilde{\varphi}_i\,,$$

where $e_i\tilde{\varphi}_i$ is the energy of interaction of an ion having charge e_i with the ionic shell. Finally, representation $\mu_i = \mu_{0i} + k_B T\ln n_{0i}$ is also used, where n_{0i} is the ion concentration in a bulky liquid [67, 68].

We believe that such representations associated with different methods of approximate calculations are poorly substantiated. Therefore, we shall proceed from physical considerations. To begin with, we note that the thermodynamic functions in Eqn (40) are averaged characteristics. Indeed, Γ_i is the mean number of ith particles per unit surface area, meaning that the chemical potential μ_i must correspond to the mean particle energy in the transition layer.

Because $n_i(x)$ varies in the transition layer, the particle's chemical potential μ_i' in this layer is likewise a variable function, $\mu_i'(x)$. Ion interaction with the ionic shell in low-conducting media is insignificant; therefore, it is claimed that $\mu_i' = \mu_{0i} + k_B T \ln n_i(x)$. Then, $\mu_i = \mu_{0i} + k_B T \langle \ln n_i(x) \rangle$, where angle brackets denote averaging over the transition layer. The use of relation (32) leads to $\langle \ln n_i(x) \rangle = \ln n_0 - U_i/k_B T$, where $U_i = \langle \Pi_i(x) \rangle$ is the averaged potential. Thus, $k_B T \partial \mu_i/\partial n_0 = k_B T/n_0 - \partial U_i/\partial n_0$ and Gibbs relation (40) is written out as

$$\frac{\partial \alpha}{\partial n_0} = -k_B T \sum_i \Gamma_i \left(\frac{1}{n_0} - \frac{1}{k_B T} \frac{\partial U_i}{\partial n_0} \right). \tag{41}$$

In the case of weakly conducting fluids, the DEL may be macroscopic in size, which makes the use of relation (40) for calculating Γ_i incorrect. Therefore, we assume the thickness of the transition layer to be δ_s, which is, first, much smaller than the external characteristic size (jet or droplet radius, perturbation wavelength, etc.) and, second, not smaller than the thickness of the transition layer (a few molecular layers) in a pure fluid [66]. Under these circumstances, one obtains

$$\Gamma_i = n_0 \int_{r_0}^{\delta_s} \left[\exp\left(-\frac{\Pi_i(x)}{k_B T} \right) - 1 \right] \mathrm{d}x, \tag{42}$$

where r_0 is the effective size of a fluid molecule (ion).

Integrating Eqn (41) yields the final expression for α:

$$\alpha = \alpha_0 + \delta\alpha, \tag{43}$$

$$\delta\alpha = k_B T \sum_{i=1}^{2} \int_0^{n_0} F_i(n_0) \left(1 - \frac{n_0}{k_B T} \frac{\partial U_i}{\partial n_0} \right) \mathrm{d}n_0,$$

$$F_i(n_0) = \int_{r_0}^{\delta_s} \left[1 - \exp\left(-\frac{\Pi_i(x)}{k_B T} \right) \right] \mathrm{d}x,$$

where α_0 is the surface tension coefficient of pure liquid.

Thus, the question of the influence of impurities and external fields on surface tension reduced to the computation of mean force potential $\Pi_i(x)$. Generally speaking, parameter δ_s remains undetermined. It follows from physical considerations that $\delta_s \gg r_0$. For dilute electrolyte solutions, δ_s is assumed to be the Debye radius: $\delta_s = r_D$ [69]. In the case of weakly conducting media, δ_s may be a function of the perturbation wavelength λ. Thus, the value of δ_s for $\lambda \leqslant r_D$ depends on the transition layer thickness in a pure liquid, and then the electric field does not influence surface tension. For $\lambda \gg r_D$, it should be supposed that $\delta_s = r_D$; the electric field then has a strong effect on surface tension. The calculations are carried out in terms of the bi-ion conduction model (31) in the approximation of $\lambda \gg r_D$. Then, the averaged potentials U_i are unrelated to n_0, and the following expressions hold for $\delta\alpha$:

$$\delta\alpha = -\alpha_* F(\eta), \qquad \alpha_* = 2 k_B T r_D n_0, \tag{44}$$

$$F(\eta) = I_1(\eta) + I_2(\eta), \qquad I_1(\eta) = \int_0^{\infty} \left(\exp \Phi(s) - 1 \right) \mathrm{d}s,$$

$$I_2(\eta) = \int_0^{\infty} \left[\exp\left(-\Phi(s) \right) - 1 \right] \mathrm{d}s.$$

Because $F(\eta)$ is a positive monotonically growing function, it follows from formulas (44) that the electric field reduces surface tension. When $\eta \gg 1$, the following asymptotics takes place: $F(\eta) = 2\eta$; therefore, in strong electric fields [70]

$$\delta\alpha = -2\eta\alpha_*, \tag{45}$$

i.e., surface tension decreases in a linear fashion. This effect can be attributed to the fact that the electric field 'pulls out' ions to the surface, which results in positive adsorption and, therefore, in reduced surface tension. Notice that this result has an obvious limitation, because the ions were assumed to be structureless and the short-range forces conditioned only by the polarization interaction (33). In the general case, it is necessary to take account of dispersion forces, hydrogen bonding, etc. For example, hydrogen bonds are responsible for concentrating the alcohol molecules in the form of adsorption layers on the water surface in aqueous alcoholic solutions, where they are oriented so that the OH group is directed to the water interior [66].

In conclusion, let us provide estimates. In nonpolar liquid dielectrics at the above typical values and room temperatures, one has $\alpha_* \sim 1.8 \times 10^{-8}$ N m^{-1}. In strong electric fields ($E_n \sim 1$ MV cm^{-1}), $\eta \sim 1.3 \times 10^5$ and $\delta\alpha = -4.8 \times 10^{-3}$ N m^{-1}. Since typical α values for nonpolar dielectrics are on the order of 2×10^{-2} N m^{-1} (e.g., $\alpha \sim 0.029$ N m^{-1} for benzene), it can be concluded that the influence of an electric field on surface tension at room temperature is insignificant. Because α decreases with increasing temperature as $\alpha = \alpha_0(1 - T/T_c)$, an electric field may have an appreciable effect in the range of critical temperatures T_c.

4. Main types of EHD models

The ohmic model of electrical conduction was most commonly employed in early research on EHD effects [1, 2, 17, 18]. It still remains popular. The revision of this approach dates to the work of Felici's group [3–6]; it has been continued by many other researchers (see Refs [12, 13, 22–26]). These studies gave grounds to believe that the development of EHD flows is promoted by dissociation–injection conduction under nonequilibrium conditions of electrochemical reactions. It appears appropriate to discuss criteria for the applicability of the ohmic conduction model and to consider the most adequate models of dissociation–injection conduction.

4.1 Ohmic conduction model

Introducing volume charge density $q = \sum_i e_i n_i$ and neglecting diffusion, from Eqn (19) follows (with account of $\sum_i e_i \dot{\xi}_i = 0$) the total current balance equation

$$\frac{\partial q}{\partial t} + \operatorname{div}(\mathbf{j}^* + q\mathbf{V}) = 0, \qquad \mathbf{j}^* = \sigma \mathbf{E}, \qquad \sigma = e \sum_i b_i n_i. \tag{46}$$

These relations define the ohmic conduction law. Evidently, the ohmic conduction coefficient is a variable function given by equations (19). σ is a function of temperature and the electric field strength only in the case of equilibrium of dissociation–recombination reactions [24]:

$$\sigma = \sigma(T, E) = \sigma_0 \sqrt{F(p)}, \qquad p = \frac{e^2}{k_B T} \left(\frac{E}{4\pi\varepsilon\varepsilon_0 e} \right)^{1/2}, \tag{47}$$

where σ_0 is the field-independent conductivity in a linear section of VAC, and $F(p)$ is the Onsager factor [24].

Table 1. Values of β_σ for typical nonpolar dielectrics [71].

Liquid	$\sigma_0 \times 10^{12}\ \Omega^{-1}\ \mathrm{cm}^{-1}$	β_σ, K^{-1}	T_0, °C
Transformer oil	430 21	0.22 0.076	25
Capacitor oil	3.9 0.5 0.03	0.088 0.075 0.022	25

In studies of EHD motion in weakly nonuniform fields (in plane or spherical geometry; see Section 7) at small temperature gradients and medium field strengths of 1–10 kV cm^{-1}, it is possible to expand expression (47) into a series, confining oneself only to linear terms:

$$\sigma = \sigma_0\left[1 + \beta_\sigma(T - T_0) + \beta_E E\right], \tag{48}$$

where T_0 is the initial (e.g., ambient) temperature, and coefficient $\beta_E = e^3/[16\pi\varepsilon\varepsilon_0(k_\mathrm{B}T)^2]$.

A rise in conductivity with increasing temperature and field strength is due to the activation mechanisms of ion motion and enhanced dissociation of ion pairs. Coefficient β_σ decreases with decreasing conductivity; for nonpolar liquids, $\beta_\sigma \sim 5 \times 10^{-2}\ \mathrm{K}^{-1}$ (Table 1). In nonpolar liquids ($\varepsilon \sim 2$) at room temperature ($T \sim 300$ K), β_E takes the estimated value $2.4 \times 10^{-7}\ \mathrm{m\ V}^{-1}$.

For weak temperature inhomogeneity, dielectric constant can be represented in the form of linear dependence:

$$\varepsilon = \varepsilon_{(0)}\left[1 - \beta_\varepsilon(T - T_0)\right], \tag{49}$$

where $\varepsilon_{(0)} = \varepsilon(T_0)$. β_ε values are much lower than those of β_σ: $\beta_\varepsilon \sim 5 \times 10^{-3}\ \mathrm{K}^{-1}$. By way of example, for hexane C_6H_{14}, nitrobenzene $C_6H_5NO_2$, and ethanol C_2H_5OH at 25 °C, $\beta_\varepsilon = 8.2 \times 10^{-4}\ \mathrm{K}^{-1}$, $\beta_\varepsilon = 2.25 \times 10^{-3}\ \mathrm{K}^{-1}$, and $\beta_\varepsilon = 6.2 \times 10^{-3}\ \mathrm{K}^{-1}$, respectively [72].

The applicability criterion of the ohmic conduction model can be formulated in the following way. Experimental [71, 73] and theoretical [23–25, 53, 74–76] studies demonstrated the formation of near-electrode nonequilibrium dissociation–recombination reaction zones, the thickness of which is given by the relation [25, 76]

$$\xi_\mathrm{d} = f(n_\mathrm{i})\,\varepsilon\varepsilon_0 E_0 \frac{b_1 + b_2}{\sigma}, \tag{50}$$

where σ is the ohmic conduction coefficient [47], and $f(n_\mathrm{i})$ is a monotonically growing factor depending on the concentration of the injected ions at the electrode, such that in the absence of injection ($n_\mathrm{i} = 0$) it takes the value of $f(0) = 1$. In electric fields $E_0 \sim 10^5\ \mathrm{V\ m}^{-1}$, when $f(n_\mathrm{i}) \sim 1$, for nonpolar dielectrics ($\varepsilon \sim 2$) with typical conductivity $\sigma \sim 10^{-11}\ \Omega^{-1}\ \mathrm{m}^{-1}$ and ion mobility $b_1 \sim b_2 \sim 10^{-8}\ \mathrm{m^2\ V^{-1}\ s^{-1}}$, one obtains $\xi_\mathrm{d} = 0.2$ mm. This estimate suggests that the size of the nonequilibrium zones is commensurate with the electrode spacing d, which implies the following criterion: the ohmic conduction model (46), (47) is valid for

$$\xi_\mathrm{d} \ll d, \tag{51}$$

while the dissociation–injection model for $\xi_\mathrm{d} \geqslant d$.

The ohmic conduction model is usually realized in flat capacitors at a rather large electrode spacing d ($d \geqslant 1$ cm) and a relatively low field strength $E \sim 1$ kV cm^{-1}. Under these conditions, the results of theoretical studies [e.g., on thermo-electrohydrodynamic (TEHD) instability of an inhomogeneously heated liquid dielectric layer] [61, 77–79] fairly well describe experimental data [78, 79]. However, at small (a few millimeters) d, when the near-electrode layers begin to influence bulk processes, the TEHD-instability picture changes sharply. For example, the critical field voltage U_* may be independent of the electrode spacing [71]. In this case, the EHD flow may be related to the development of perturbations (electrothermics) in the near-electrode layers.

In strongly nonuniform high-voltage fields arising in systems with tapered electrodes (needles, blades, etc.), characteristic ξ_d values compare with electrode spacings. Thus, EHD flows in these cases practically always develop under conditions of dissociation–injection conduction.

4.2 Multiion dissociation–injection models

In the presence of injection of similarly charged ions from an electrode, and taking account of bi-ion impurity conduction, EHD processes are described by a multiion model constructed in the following way. The impurity conduction shows its worth due to decomposition of ion pairs and recombination of impurity ions, for instance, according to reactions (31). In a three-ion conduction model, the injection process occurs at a single electrode, e.g., a cathode, as a result of a reduction reaction $\mathrm{X} + \mathrm{e}^- \leftrightarrow \mathrm{X}^-$, with X^- ions being injected recombining with impurity A^+ ions in accordance with the reaction

$$\mathrm{X}^- + \mathrm{A}^+ \xrightarrow{\alpha_1} \mathrm{X^-A^+} \rightarrow \mathrm{X} + \mathrm{A}, \tag{52}$$

where α_1 is the pair recombination coefficient of A^+ and X^- ions. In this case, one has a three-ion model in which sources $\dot{\xi}_i$ are defined as

$$\dot{\xi}_1 = \dot{\xi}_2 + \dot{\xi}_4, \quad \dot{\xi}_2 = k_\mathrm{d}N - \alpha_{11}n_1n_2, \quad \dot{\xi}_4 = -\alpha_1 n_1 n_4, \tag{53}$$

where n_1, n_2, and n_4 are the concentrations of A^+, B^-, and X^- ions, respectively, and N is the concentration of $\mathrm{A^+B^-}$ ion pairs. Such a model can describe, for instance, EHD flows in nonpolar liquid dielectric solutions with an electron acceptor, such as molecular iodine I_2 [80, 81].

Molecules of polar dielectrics always containing an electronegative atom or a group are denoted as R–X, where R is the radical (e.g., a benzene ring in hydrogen halides), and X is the electron acceptor [44, 45]. In this case, the liquid may undergo ionization by virtue of thermal autodissociation:

$$\mathrm{R{-}X} \leftrightarrow \mathrm{X{-}R^+ + R{-}X^-}. \tag{54}$$

Such liquids are exemplified by hydrogen halides (chlorobenzene, bromobenzene, iodobenzene), alcohols, nitrobenzene, and some others. It should be noted that, unlike the conductivity of nonpolar dielectrics, which can be lowered by ultrapurification to $\sigma = 10^{-19}\ \Omega^{-1}\ \mathrm{cm}^{-1}$ [19], that of polar liquid dielectrics drops only to $\sigma = 10^{-13}\ \Omega^{-1}\ \mathrm{cm}^{-1}$ and increases with time thereafter due to autodissociation to $\sigma = (10^{-10} - 10^{-11})\ \Omega^{-1}\ \mathrm{cm}^{-1}$ [3, 5]. In strong electric fields, polar molecules participate in electrochemical redox reactions according, for instance, to the following schemes [45, 46]:

$$\mathrm{R{-}X} + \mathrm{e}^-(\mathrm{M}) \leftrightarrow \mathrm{R{-}X^-} \text{ at the cathode}, \tag{55}$$

$$\mathrm{R{-}X} \leftrightarrow \mathrm{R{-}X^+} + \mathrm{e}^-(\mathrm{M}) \text{ at the anode}, \tag{56}$$

where $\mathrm{e}^-(\mathrm{M})$ is an electron in the metal.

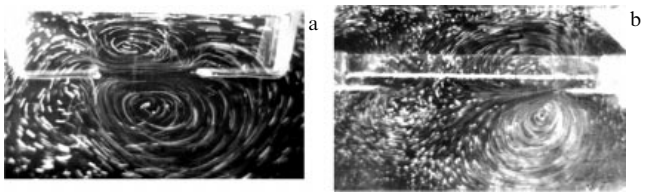

Figure 4. EHD flows in symmetric systems of electrodes imbedded in iodine-containing transformer oil solutions [80, 81]: (a) a system of two parallel wires, and (b) a blade–blade electrode system. In either case, the flow is directed from the negative electrode.

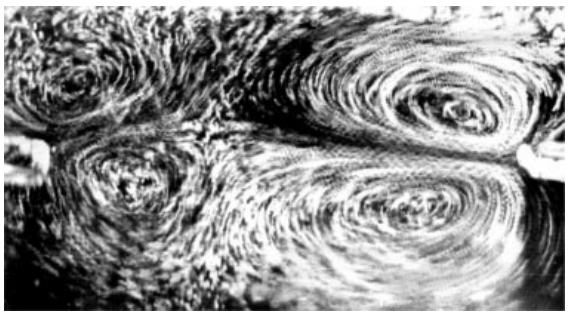

Figure 5. The four-cell structure of an EHD flow in polar liquids (bromobenzene, chlorobenzene, etc.) in a system of two parallel wires [82]. Bigger vortices form near the negative electrode.

The presence of (55), (56) type reactions is easy to verify by the streamline fixation method in EHD flows [77] (Fig. 4). In polar dielectrics, cathode injection proceeds normally more intense than the anode one. It is evidenced not only by the EHD flow data (Fig. 5) but also by the measurements of electric field strength distributions using the Kerr effect [82, 83].

Multiion conduction models with an arbitrary number of ions can be constructed in a similar way, although even a three-ion model allows all characteristic patterns of electrochemical processes to be elucidated. For example, the seemingly 'threshold' nature of the development of EHD flows in an asymmetric electrode system, when equilibrium conditions are not satisfied, can be accounted for by the switch-over of the dissociation conduction mode to the injection one [53]. Moreover, this model takes account of the influence of technical (uncontrollable) impurities (like iodine, butyl alcohol, etc.) on the injection conduction. Further development of the three-ion model entails an in-depth study of injection processes responsible for the intensity of EHD flows and the enhancement of EHD-system performance resources.

4.3 EHD equations in alternating external fields

In order to balance electrical conduction effects, it is possible to apply alternating external fields of a sufficiently high frequency (the high-frequency EHD approximation). As shown in Ref. [84], EHD flows in liquid dielectrics with conductivity $\sigma \sim 10^{-12}\ \Omega^{-1}\ \mathrm{cm}^{-1}$ damp out at frequencies $\omega \geqslant 1$ kHz, even for spiked electrodes. The order of frequency at which an EHD flow ceases can be determined in the following way.

Suppose that an EHD flow develops as a result of charge injection. The size of the near-electrode region δ_i, where the bulk charge accumulates, depends on the migration displacement of ions during the oscillation half-period, i.e., $\delta_\mathrm{i} = b_\mathrm{i}E/2\omega$, where b_i is the mobility of the ions being injected. At typical values of $b_\mathrm{i} = 10^{-8}\ \mathrm{m^2\ V^{-1}\ s^{-1}}$ in the case of spiked electrodes ($E \sim 10^7\ \mathrm{V\ m^{-1}}$) and frequencies $\omega = 50\ \mathrm{s^{-1}}$, one finds $\delta_\mathrm{i} = 1$ mm. This means that the migration motion of ions at industrial frequencies charges only a narrow near-electrode region. The ion displacement δ_h due to the EHD flow is expressed in a similar way: $\delta_\mathrm{h} = V/2\omega$, where the developing flow rate is found from the momentum equation $\rho\,\partial V/\partial t \sim qE$, i.e., over the course of half-period: $V \sim qE/2\rho\omega$. Assuming $q = en_\mathrm{i}$ at the typical values of $n_\mathrm{i} = 10^{11}\ \mathrm{cm^{-3}}$, $E \sim 10^5\ \mathrm{V\ cm^{-1}}$, $\rho = 1\ \mathrm{g\ cm^{-3}}$, and $\omega = 50\ \mathrm{s^{-1}}$, we obtain $V \sim 1.6\ \mathrm{m\ s^{-1}}$, i.e., $\delta_\mathrm{h} \sim 1.6$ cm. Hence it follows that at industrial frequencies the liquid in a large part of the interelectrode region is charged due to EHD convection, and only for $\omega \geqslant 1$ kHz it is charged in the narrow near-electrode region, thus accounting for the damping of the EHD flow.

Certainly, this is only a rough estimate, but the rate $V \sim 1\ \mathrm{m\ s^{-1}}$ is typical of EHD flows in the system of spike electrodes [11–13, 85]. Therefore, the condition of the absence of an EHD flow during charge injection can be written down as

$$\max\left(\delta_\mathrm{i}, \delta_\mathrm{h}\right) \ll d\,, \qquad \delta_\mathrm{i} = \frac{b_\mathrm{i}E}{2\omega}\,, \qquad \delta_\mathrm{h} = \frac{qE}{4\rho\omega^2}\,. \tag{57}$$

The high-frequency region is dominated by polarization forces, especially in the case of thermal inhomogeneity. This effect is utilized to model atmosphere dynamics in a laboratory setup consisting of embedded spheres rotating relative to each other [86]. At sufficiently small interelectrode gaps in the medium field region (1–10 kV cm^{-1}), the ohmic conduction model (46), (47) can be used as a basis, which poses a number of questions pertaining to the choice of the frequency. Indeed, at high enough frequencies dielectric loss shows its worth, while a frequency drop gives rise to pulsation forces associated with the ohmic conduction gradient; hence, the necessity of deriving averaged EHD equations in high-frequency fields.

The averaged equations are convenient to derive in dimensionless variables by the method described in well-known monograph [87]. Let us assume that the Boussinesq approximation is fulfilled [88], while medium electrical conduction and polarization are given by linear relations (48), (49). Let us further choose the following quantities as measurement units: $[t] = 1/\omega$, $\left[|r|\right] = d$, $\left[|V|\right] = V_0 = \eta/\rho d$, $[p] = \rho V_0^2$, $[\Phi] = U$, $[q] = \varepsilon_{(0)}\varepsilon_0 E_0/d$ $(E_0 = U/d)$, and $[T] = \delta T$, where d is the interelectrode gap, U is the voltage across the electrodes, and $\delta T = |T_2 - T_1|$ is the temperature difference between the electrodes. In dimensionless variables, the system of EHD equations is written out in the form

$$\mathrm{St}\,\frac{\partial \mathbf{V}}{\partial t} + (\mathbf{V}\nabla)\mathbf{V} = -\nabla p + \Delta\mathbf{V} - Gq\nabla\Phi - 0.5G\beta_\varepsilon^*\varepsilon_{(0)}|\nabla\Phi|^2\nabla T + RT\mathbf{e}_z\,, \tag{58}$$

$$\mathrm{div}\,\mathbf{V} = 0\,, \qquad \mathrm{St}\,\frac{\partial q}{\partial t} + \mathrm{div}\left(-\Pi_\mathrm{e}\tilde{\sigma}\nabla\Phi + q\mathbf{V}\right) = 0\,, \qquad \mathrm{div}\left(\tilde{\varepsilon}\nabla\Phi\right) = -q\,, \tag{59}$$

$$\mathrm{St}\,\frac{\partial T}{\partial t} + \mathbf{V}\nabla T = \Pi\Delta T + I_\mathrm{d}\tilde{\varepsilon}|\nabla\Phi|^2\,, \tag{60}$$

$$\varepsilon_{(0)} = \varepsilon(T_1)\,, \qquad \tilde{\sigma} = 1 + \beta_E^*|\nabla\Phi| + \beta_\sigma^* T\,, \qquad \tilde{\varepsilon} = 1 - \beta_\varepsilon^* T\,.$$

The dimensionless parameters are given by the expressions

$$\mathrm{St}=\frac{\omega d}{V_0}\,,\qquad G=\frac{\varepsilon_{(0)}\varepsilon_0 E_0^2}{\rho_0 V_0^2}\,,\qquad R=\frac{\beta_\rho^* g d}{V_0^2}\,,$$

$$I_\mathrm{d}=\frac{\omega\varepsilon_{(0)}\varepsilon_0 E_0^2 d}{2\rho_0 c_p\,\delta T\,V_0}\tan\varphi\,,\qquad \Pi=\frac{\lambda}{c_p\eta}\,,\qquad \Pi_\mathrm{e}=\frac{d}{\tau_\mathrm{e}V_0}\,,$$

$$\tau_\mathrm{e}=\frac{\varepsilon_{(0)}\varepsilon_0}{\sigma_0}\,,\qquad \beta_E^*=\beta_E E_0\,,\qquad \beta_\sigma^*=\beta_\sigma\,\delta T\,,$$

$$\beta_\varepsilon^*=\beta_\varepsilon\,\delta T\,,\qquad \beta_\rho^*=\beta_\rho\,\delta T\,.$$

They take into account dielectric losses (13); β_ρ is the thermal expansion coefficient for the fluid:

$$\rho=\rho_0\bigl[1-\beta_\rho(T-T_1)\bigr]\,,$$

λ is the thermal conductivity coefficient, c_p is the heat capacity per unit mass, η is the coefficient of dynamic viscosity, and $\mathbf{e}_z$ is the unit vector directed against gravity.

The boundary conditions in dimensionless variables acquire the form

$$\begin{aligned}&\mathrm{S}_1\ (\text{anode}):\quad \Phi=\cos t\,,\ V=0\,,\ T=1;\\ &\mathrm{S}_2\ (\text{cathode}):\quad \Phi=0\,,\ V=0\,,\ T=0\,.\end{aligned}\tag{61}$$

The high-frequency approximation is defined by the condition $\mathrm{St}\gg 1$. By introducing the small parameter $\mu=1/\mathrm{St}$, the solution is sought in the form

$$\begin{aligned}&\mathbf{V}=\mathbf{u}+\mathbf{V}'\,,\quad p=p_\mathrm{c}+p'\,,\\ &\Phi=\Phi_0\cos t+\Phi'\,,\quad T=\Theta+T'\,,\end{aligned}\tag{62}$$

where $\mathbf{u}=\mathbf{u}(\tau,\mathbf{r})$, $\Theta=\Theta(\tau,\mathbf{r})$ are the mean velocity and temperature, the prime denotes pulsation functions of order μ, and $\tau=\mu t$ is the slow time. The averaging operation is defined as

$$\mathbf{u}=\langle\mathbf{V}\rangle=\frac{1}{\mathrm{St}}\int_0^{\mathrm{St}}\mathbf{V}(t,\mathbf{r})\,\mathrm{d}t\,,\qquad \mathrm{St}\gg 1\,.$$

In what follows, calculations are made for the case of low dielectric heating, $I_\mathrm{d}\ll 1$, and weak temperature differential δT, interesting in terms of applications. These assumptions imply the smallness of parameters β_ρ^*, β_ε^*, β_σ^* and the finiteness of frequencies:

$$\omega\ll\omega_2=\frac{2\rho_0 c_p\,\delta T\,V_0}{\varepsilon_{(0)}\varepsilon_0 E_0^2 d\tan\varphi}\,.\tag{63}$$

By way of example, for transformer oil [89] under simulation conditions [86] at

$$\begin{aligned}&T_0=20\,^\circ\mathrm{C}\,,\quad \rho_0=880\ \mathrm{kg\ m^{-3}}\,,\quad \lambda=0.111\ \mathrm{W\ m^{-3}\ K^{-1}}\,,\\ &c_p=1.7\ \mathrm{kJ\ kg^{-1}\ K^{-1}}\,,\quad \eta=0.021\ \mathrm{N\,s\ m^{-2}}\,,\quad \delta T=5\,^\circ\mathrm{C}\,,\\ &d=5\ \mathrm{cm}\,,\quad \varepsilon_{(0)}=2.2\,,\quad \tan\varphi=0.02\,,\quad E_0=10\ \mathrm{kV\ cm^{-1}}\,,\end{aligned}\tag{64}$$

it was found that $\omega_2=34$ kHz, and for $\omega\leqslant 1$ kHz the inequality $I_\mathrm{d}\ll 1$ is fulfilled.

In the framework of the above assumptions, temperature pulsations may be disregarded. Substituting formulas (62) into Eqns (58)–(60) and averaging them yield the following averaged equations

$$\frac{\partial\mathbf{u}}{\partial\tau}+(\mathbf{u}\nabla)\mathbf{u}=-\nabla p_\mathrm{c}+\Delta\mathbf{u}+\mathbf{f}_\mathrm{p}-\mu^2\mathbf{f}_\omega+RT\mathbf{e}_z\,,\quad \mathrm{div}\,\mathbf{u}=0\,,\tag{65}$$

$$\frac{\partial T}{\partial\tau}+\mathbf{u}\nabla T=\Pi\Delta T\,,\tag{66}$$

where $\mathbf{f}_\mathrm{p}$ and $\mu^2\mathbf{f}_\omega$ are the polarization and pulsation forces defined in the $\beta_\varepsilon^*\ll\beta_\sigma^*\ll 1$ approximation as

$$\begin{aligned}&\mathbf{f}_\mathrm{p}=0.5G\beta_\varepsilon^*\varepsilon_{(0)}E_0^2\nabla T\,,\\ &\mathbf{f}_\omega=0.5\Pi_\mathrm{e}\beta_\sigma^*\bigl[Gq_{(2)}\mathbf{E}_0+2\Pi_\mathrm{e}(\mathbf{E}_0\mathbf{E}_{(2)})\nabla T\bigr]\,.\end{aligned}\tag{67}$$

Here, $\mathbf{E}_0=-\nabla\Phi_0$, $\mathbf{E}_{(2)}=-\nabla\Phi_{(2)}$, $q_{(2)}=\mathbf{E}_0\nabla T-\nabla(\mathbf{E}_0\nabla T)\mathbf{u}$, and potentials Φ_0, $\Phi_{(2)}$ are given by equations $\mathrm{div}\,(\tilde{\varepsilon}\nabla\Phi_0)=0$, $\mathrm{div}\,(\tilde{\varepsilon}\nabla\Phi_{(2)})=q_{(2)}$ at the boundary conditions S_1 — $\Phi_0=1$, $\Phi_{(2)}=0$, and S_2 — $\Phi_0=\Phi_{(2)}=0$.

Let us estimate the parameters at which polarization forces predominate. For highly purified fluids with $\sigma_0=10^{-14}\ \Omega^{-1}\ \mathrm{cm}^{-1}$ at the parameters specified in Eqn (64) and typical values of $\beta_\sigma=0.02\ \mathrm{K}^{-1}$, $\beta_\varepsilon=0.001\ \mathrm{K}^{-1}$, polarization forces dominate for $\mu^2\Pi_\mathrm{e}^2\beta_\sigma\ll\varepsilon_{(0)}\beta_\varepsilon$, or

$$\omega\gg\omega_1=\frac{1}{\tau_\mathrm{e}}\sqrt{\frac{\beta_\sigma}{\varepsilon_{(0)}\beta_\varepsilon}}\,,\qquad \tau_\mathrm{e}=\frac{\varepsilon_{(0)}\varepsilon_0}{\sigma_0}\,.\tag{68}$$

For the above values, one has $\omega_1=25$ Hz. These estimates indicate that in highly purified fluids ($\sigma_0\leqslant 10^{-14}\ \Omega^{-1}\ \mathrm{cm}^{-1}$) conductivity effects are readily eliminated, even at relatively low frequencies: $\omega_1\sim 200$ Hz. However, at high conductivities, e.g., for aqueous solutions with $\sigma_0\sim 10^{-7}\ \Omega^{-1}\ \mathrm{cm}^{-1}$, the charge relaxation time is small: $\tau_\mathrm{e}\sim 10^{-6}$ s; therefore, conductivity effects manifest themselves in aqueous solutions even at high frequencies: $\omega_1\sim 10$ kHz.

5. Dimensionless criteria. EHD approximations

The multiion dissociation–injection EHD model is a many-parameter one and has a high degree of generality. This model is able to transform into different variants, the so-called EHD approximations, depending on the electric field strength, conductivity, and electrode geometry. In order to estimate the applicability of a given approximation, it is necessary to introduce dimensionless parameters (criteria) determining approximation errors.

It will suffice to derive the EHD criteria based on a three-ion model: A^+, B^- impurity ions, according to reaction (31), and X^- ions being injected that are generated in the reaction $\mathrm{X}+\mathrm{e}^-\leftrightarrow\mathrm{X}^-$ and interact with the impurity ions, in accordance with reaction (52).

Let us choose the following characteristic quantities as measurement units: interelectrode gap d for the length, voltage U across the electrodes for the potential, positive ion migration rate $V_1=b_1E_0$, $E_0=U/d$ for the velocity, d/V_1 for time, with the equilibrium concentration n_0 determined in the case of impurity ions according to formula (47) at $E_0=0$ for the concentration, the value of the injection function $n_\mathrm{c}(E_0)$ defined according to formula (23) or (25) for the ions being injected, and ρV_1^2 for the pressure. This brings up the

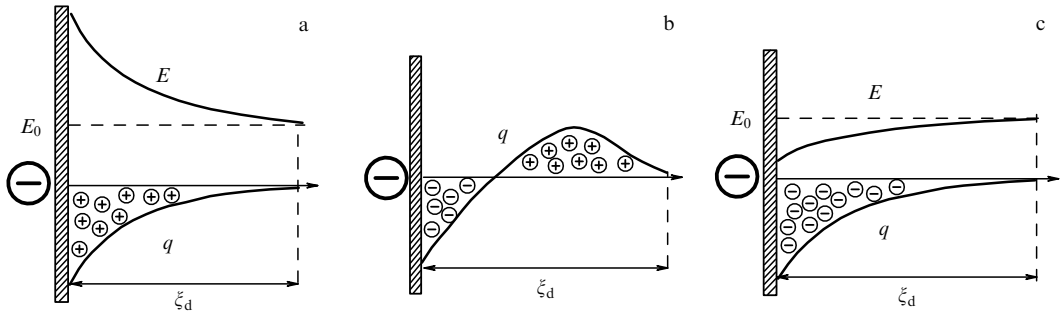

Figure 6. Formation of ionic structures in near-cathode layers: (a) weak injection, $\sigma_c \ll 1$; (b) moderate injection, $\sigma_c \sim 1$, and low mobility of the ions being injected: $b_4 \ll b_1$; (c) intense injection, $\sigma_c \gg 1$.

following set of equations in dimensionless variables that remain denoted as before:

$$\frac{\partial \mathbf{V}}{\partial t} + (\mathbf{V}\nabla)\mathbf{V} = -\nabla p' + \frac{1}{R_e}\,\Delta \mathbf{V} + CMq\mathbf{E}\,, \quad \operatorname{div}\mathbf{V} = 0; \tag{69}$$

$$\operatorname{div}\mathbf{E} = Cq\,, \quad \mathbf{E} = -\nabla\Phi\,, \quad q = n_1 - n_2 - \sigma_c n_4; \tag{70}$$

$$\frac{\partial n_j}{\partial t} + \operatorname{div}\left[(-1)^{j-1}\beta_j n_j \mathbf{E} + n_j\mathbf{V}\right] = C\dot{\xi}_j\,, \quad j = 1,2; \tag{71}$$

$$\frac{\partial n_4}{\partial t} + \operatorname{div}\left[-\beta_4 n_4\mathbf{E} + n_4\mathbf{V}\right] = C\dot{\xi}_4\,, \tag{72}$$

$$\dot{\xi}_2 = (1+\beta_2)\left[F(p) - n_1 n_2\right]\,, \quad \dot{\xi}_1 = \dot{\xi}_2 - \sigma_c n_1 n_4(1+\beta_4)\,,$$

$$\dot{\xi}_4 = -n_1 n_4(1+\beta_4)\,, \quad R_e = \frac{b_1 U}{\nu}\,, \quad \nu = \frac{\eta}{\rho}\,, \quad M = \frac{\varepsilon\varepsilon_0}{\rho b_1^2}\,,$$

$$\sigma_c = \frac{n_c(E_0)}{n_0}\,, \quad \beta_i = \frac{b_i}{b_1}\,, \quad i = 1,2,4\,, \quad C = \frac{d}{\xi_d}\,,$$

$$\xi_d = \frac{\varepsilon\varepsilon_0 E_0}{q_0}\,, \quad q_0 = en_0 = \frac{\sigma_0}{b_1 + b_2}\,.$$

For liquids, parameter $M \sim 100$ (e.g., $M = 185$ for transformer oil at room temperature), the mobility ratio $\beta_i = b_i/b_1 \leqslant 1$, whereas parameters R_e, C, σ_c may vary over broad ranges depending on voltage U, electrode spacing d, and conductivity σ_0. Parameter R_e plays the role of the Reynolds number. Parameter σ_c determines electrical conduction modes: for $\sigma_c \ll 1$, the ion injection is weak and conductivity depends on impurity ions alone, while for $\sigma_c \gg 1$ the ions being injected predominate (injection conduction mode), and at $\sigma_c \sim 1$ mixed dissociation–injection conduction is realized. Parameter C determines the strength of ion interaction: specifically, for $C \ll 1$ the ion concentration or the cell size d is so small that both the ion–ion interaction and the electric field they induce may be neglected. Conversely, for $C \gg 1$ the ions are strongly bound, and the ohmic conduction mode comes into play.

Let us consider a scenario for the development of EHD flows by the example of a flat capacitor with a large enough interelectrode gap ($d \geqslant 1$ cm). In low-voltage fields ($E_0 \leqslant 1$ kV cm^{-1}), one has $C \gg 1$. In such a case, the ion–ion interaction has a nonequilibrium character only in narrow near-electrode layers of the thickness given by formula (50). Outside the nonequilibrium layers, conductivity is a function of impurity ions strongly involved in dissociation–recombination reactions. In this region, electrohydrodynamics is described by the ohmic conduction model.

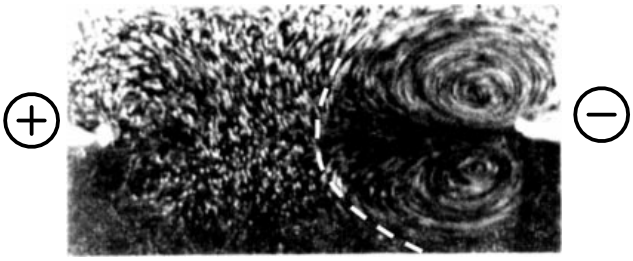

Figure 7. The development of electroconvection in a system of two parallel copper wires 1 mm in diameter [81]. The fluid is an iodine-containing transformer oil solution. The dashed line shows the border between equilibrium and nonequilibrium regions.

Mechanisms of bulk charge formation in near-electrode layers were described in Refs [25, 70]. Given the injection level is low, $\sigma_c \ll 1$, the sign of the charge of near-electrode layers is opposite to electrode polarity (such a case is described as heterocharge formation near an electrode), and the electric field strength in the vicinity of the electrodes increases (Fig. 6a). The thickness ξ of the near-electrode nonequilibrium layer also increases with the growing field due to enlargement of the nonequilibrium reaction region (31) and enhancement of ion injection. Two cases can be realized depending on the degree of ion mobility. First, a bipolar charge structure forms at low mobility and a homocharge emerges at the electrode surface (Fig. 6b). As the electric field grows further, bipolar structures disappear and the near-electrode region becomes homocharged, while the electric field near the electrode decreases in strength (Fig. 6c). As the field increases still further, the near-electrode layers lose stability, which promotes the development of EHD flows (Fig. 7). In this field strength region, the EHD flows are described by the multiion dissociation–injection model.

6. Nonstationary and transient processes

We shall call an arrangement of two electrodes with a liquid dielectric in the gap between them an EHD cell. The switching-on of a high-voltage field gives rise to transient processes in the EHD cell, viz. the formation of ion waves and near-electrode ionic structures, development of EHD flows, etc. The transient processes associated with the passage of a current are divided into fast and slow. Analysis of the former was undertaken in review [25]. In the case of instantaneous switching-on of the high-voltage field, ion waves form in the cell for $C \ll 1$, and near-electrode layers for $C \gg 1$. The characteristic time of these processes is less than 1 second.

Slow transient processes frequently referred to as electropurification [19] take a few hours and even days to complete; they are accompanied by precipitation of ionic impurities on the electrodes.

A change of conduction modes associated with variations of the electric field strength is regarded as an atemporal transient process, with the key parameter being the $\sigma_c = n_c(E_0)/n_0$ ratio, where $n_c(E_0)$ is the concentration of the ions being injected and specified by the injection function, and n_0 is the concentration of impurity ions. Because $n_c(E_0)$ is a monotonically growing function of the field strength, it turns out that $\sigma_c \ll 1$ in low fields and conductivity is determined by impurity ions; for $\sigma_c \gg 1$ it depends on injection ions.

When the injection of charges predominates, the crucial role in the development of EHD flows is played by nonlinear ion waves, which will be considered in greater detail in Section 6.1.

6.1 Nonlinear ion waves

Usually, charges are either injected into a fluid from the outside or generated inside it under the effect of ionizing radiation. As a rule, they are distributed in the process nonuniformly, which, in turn, brings into existence EHD instability of the liquid and, as a consequence, may result in large inaccuracies in the measurement of b_i [90]. EHD instability of ion waves affects not only the structure of EHD flows but also discharge formation pattern associated with an electric breakdown in the fluid [23]. This poses the problem of investigation into the motion of a unipolarly charged ion cloud in the nonlinear formulation and its stability. These issues are dealt with in the following order: first, the problem of ion motion in a quiescent fluid is solved, and then EHD instability is analyzed.

The motion of a cloud of positive charges in a quiescent fluid of infinite extent is described by the following boundary value problem:

$$\varepsilon\varepsilon_0 \operatorname{div} \mathbf{E} = q\,, \qquad q_t + b \operatorname{div}(q\mathbf{E}) = 0; \tag{73}$$

$$t = 0\colon \quad q = q_0\,, \quad \mathbf{E} = \mathbf{E}_{(0)}; \quad |\mathbf{r}| \to \infty\colon \quad \mathbf{E} \to \mathbf{E}_0 + \mathbf{E}_i\,. \tag{74}$$

From here on, subscript t denotes the partial time derivative, q_0 is the initial volume charge distribution, and $\mathbf{E}_{(0)}$ is the initial strength of the field formed by external field $\mathbf{E}_0$ and charge q_0-induced field $\mathbf{E}_i$.

Principal motion patterns of the charge cloud can be illustrated by the example of a $2d$-thick flat layer at $q_0 = \text{const}$ and an external field oriented normally to it. In this case, it is possible to rely on the approximation $E_i = q_0 d/\varepsilon\varepsilon_0 \ll E_0$, $t \ll \tau_e = \varepsilon\varepsilon_0/bq_0$ for finding the exact solution [25, 91], which is not presented here. We shall study EHD instability of an ion layer in this approximation (q_0 is the mean charge density) at an arbitrary, in general, distribution of the unperturbed charge within the layer, $q_{(0)} = q_{(0)}(x)$, where the origin of the x coordinate lies in the middle of the layer, and the x-axis is directed across it. In this event, the equations for small perturbations in a system of coordinates traveling with the layer are written down in the form

$$\rho \mathbf{V}_t = -\nabla p + \eta \Delta \mathbf{V} + q\mathbf{E}_0\,, \qquad \operatorname{div} \mathbf{V} = 0\,,$$
$$q_t = -q_0' V_x\,, \qquad q_0' = \frac{\mathrm{d}q_{(0)}}{\mathrm{d}x}\,, \tag{75}$$

where V_x is the x-component of the velocity.

The boundary conditions are given by the continuity of the velocity and the viscous stress tensor at the borders of the layer and by the damping of perturbations at infinity.

We use Lyapunov's first method to study instability, assuming $\mathbf{V} = \mathbf{V}(\mathbf{r}) \exp(\lambda t)$, where λ is the spectral parameter to be determined. The motion of the ion cloud is unstable for $\operatorname{Re}\lambda > 0$, and stable as $\operatorname{Re}\lambda \leqslant 0$ for any initial perturbations. The quantity $\delta_r = \operatorname{Re}\lambda$ is called the perturbation buildup decrement. An arbitrary perturbation being the superposition of normal modes, suffice it to study stability relative to a single mode: $\mathbf{V}(\mathbf{r}) = \mathbf{V}(x) \exp[\mathrm{i}(k_y y + k_z z)]$, where y, z are the Cartesian coordinates orthogonal to the x-axis. Elementary transformations with respect to component $V = V_x$ lead to the following problem on eigenvalues of λ:

$$\lambda(\eta \hat{L}^2 V - \rho\lambda \hat{L} V) = -E_0 q_0' k^2 V; \tag{76}$$

$$x = \pm d\colon \quad \langle V \rangle = \langle V' \rangle = \langle V'' \rangle = \langle V''' \rangle = 0\,, \qquad |x| \to \infty\colon \quad V \to 0\,, \tag{77}$$

where $\hat{L} = \mathrm{d}^2/\mathrm{d}x^2 - k^2$, $k^2 = k_y^2 + k_z^2$, and E_0 is the projection of $\mathbf{E}_0$ onto the x-axis.

Multiplying Eqn (76) by the complex conjugate function V^* and integrating from $x = -\infty$ to $x = +\infty$ with account of boundary conditions (77) lead to the conclusion that instability develops for $q_0' > 0$, suggesting that the ion cloud is unstable when the charge gradient decreases along the direction of charge motion, $\nabla q_0 \uparrow\downarrow \mathbf{E}_0$, and stable in the opposite case, $\nabla q_0 \uparrow\uparrow \mathbf{E}_0$ [91].

Problem (76), (77) may be studied in the analytical form at $q_0' = \text{const}$. Introducing dimensionless parameters $p = \lambda d^2/\nu$, $\nu = \eta/\rho$, $B = -q_0' E_0 d^4/\nu\eta$, and $\kappa = kd$, we find that the spectral parameter p is defined by the following equations:

$$|r_4| \tan |r_4| + r_3 \tanh r_3 = 0\,, \qquad |r_4| \cot |r_4| + r_3 \coth r_3 = 0\,,$$
$$r_3 = \left(\kappa^2 + \frac{p}{2} + \sqrt{\frac{\kappa^2 B}{p} + \frac{p^2}{4}}\right)^{1/2}, \tag{78}$$
$$|r_4| = \left(\sqrt{\frac{\kappa^2 B}{p} + \frac{p^2}{4}} - \kappa^2 - \frac{p}{2}\right)^{1/2}.$$

The first and second equations correspond to symmetric and asymmetric perturbations, respectively. The analysis of equations (78) indicates that the parameter p is bounded from above: $p < p_* = \sqrt{\kappa^4/4 + B} - \kappa^2/2$. Using this inequality, it is possible to prove that in high-viscous media or small charge density and field gradients ($B \ll 1$), instability takes place only in the case of asymmetric perturbations, with the spectral parameter λ for $4B \ll \kappa^4$ being expressed as

$$\lambda = -0.08 q_0' \frac{E_0 l^2}{\eta}\,, \qquad B \ll 1\,, \tag{79}$$

where $l = 2\pi/k$ is the perturbation wavelength. This means that long-wave perturbations grow especially fast.

In the limiting case of low-viscous media or high fields and large volume charge gradients ($B \gg 1$) for $\kappa^2 \ll B^{1/2}$, the sought spectral parameter is given by

$$\lambda = \frac{\sqrt{-q_0' E_0/\rho}\,\kappa^2}{\kappa^2 + \zeta}\,, \qquad B \gg 1\,, \tag{80}$$

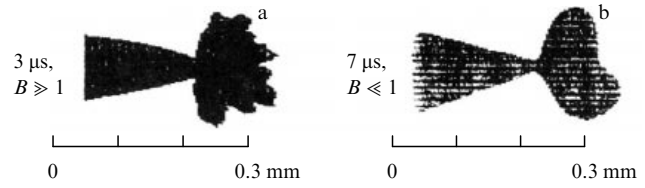

Figure 8. Shadow pictures illustrating the development of EHD instability of ion clouds in a DC-200 silicone fluid [23] near the spiked electrode: (a) low-viscous fluid, $\eta = 0.02$ St, $U = 11.5$ kV, and (b) viscous fluid, $\eta = 10$ St.

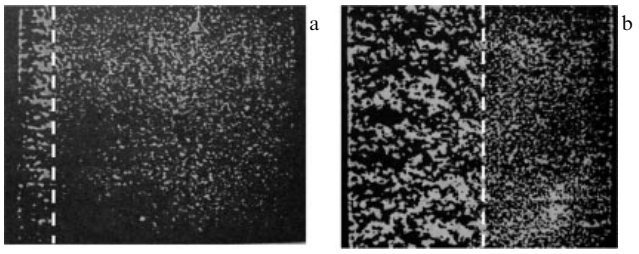

Figure 9. Shadow pictures of the development of EHD instability of ion clouds for strong unipolar charge injection [23]. The dashed line shows the border between charged (left) and uncharged regions. Interelectrode gap is 5.6 mm, $U = 18$ kV, $t = 0.95$ ms (a), and $t = 2.9$ ms (b).

where the parameter $\zeta \sim 1$. This estimate holds true for both symmetric and asymmetric perturbations, and in this case the fastest growing perturbations are those for which $\lambda \sim \sqrt{-q_0' E_0/\rho}$.

The validity of relationships (79), (80) is confirmed by numerous experimental data. Here are three of the most characteristic examples illustrating the role of instability of ion clouds in the development of EHD movements of fluids at the initial stages of unipolar charge injection.

(1) In the study of a breakdown in a spiked–plane electrode system, the charges injected from the spike drift away from the electrode in the form of an ion cloud. Its diffusion smearing at the front boundary satisfies condition $\nabla q_0 \uparrow\downarrow E_0$, i.e., the instability condition. It was shown in experiment [23] that on small time intervals ($\leqslant 3$ μs), short-wave perturbations develop in low-viscous fluids (Fig. 8a), and long-wave ones in high-viscous fluids (Fig. 8b).

(2) Strong unipolar injection of charges from the ionite membrane to nitrobenzene gives rise to EHD instability of the charge plane front, which accounts for the small-scale turbulent motion in the charged region of the fluid, while the uncharged region remains quiescent [23] (Fig. 9).

(3) In an iodine-containing transformer oil solution and a system of coaxial cylindrical electrodes with a small radius of the central electrode, the switching-on of high voltage triggers a vortical EHD flow, with the number of vortices always exceeding four [92] (Fig. 10a), in contrast to exactly four in the stationary case (Fig. 10b).

This effect is attributed to instability of the cloud of negative charges injected from the central electrode (cathode).

6.2 Alternation of conduction modes

In previous Section 6.1, we dealt with the development of transient processes in time. Variation of parameter σ_0 determining impurity conductivity gives rise to a transient process responsible for a change in the conduction mode. The

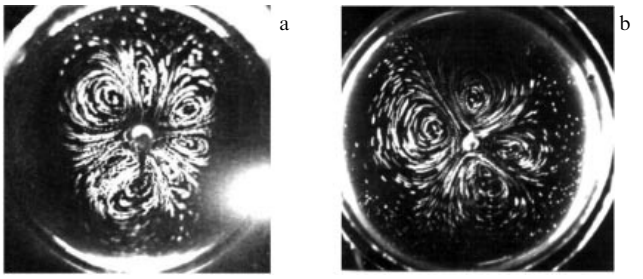

Figure 10. Flow patterns in an iodine-containing transformer oil solution [92]: (a) at the onset, and (b) in the steady state.

main features of this process are readily apparent in a flat capacitor under the conditions of the inductionless approximation and weak ion injection: $C = d/\xi_d \ll 1$, $C_i = \sigma_c C = e n_c d/(\varepsilon\varepsilon_0 E_0) \ll 1$. Then, the equilibrium field and charge distributions in the linear approximation in small parameters C and C_i in a steady state are described by the equations

$$\begin{aligned} &(-1)^{j-1}\beta_j \nabla n_{j1}\mathbf{E}_0 = (1+\beta_1)F_0\,, \quad j = 1,2\,,\\ &-\nabla n_{41}\mathbf{E}_0 = 1\,, \end{aligned} \tag{81}$$

where $\mathbf{E}_0$ is the external electric field, and $F_0 = F(p)$ at $E = E_0$.

Boundary conditions at the electrodes take the form

$$n_{11} = 0 \text{ at the anode, and } n_{21} = n_{41} = 0 \text{ at the cathode}\,. \tag{82}$$

The boundary condition for the negative charges being injected from the cathode is fulfilled in the zero approximation, while the boundary conditions for impurity ions are the consequences of the absence of the current of positive (negative) charges entering the anode (cathode).

The dimensionless volume charge is defined as

$$q_0 = C(n_{11} - n_{21}) - \sigma_c(1 + C_i n_{41})\,,$$

$$F_0 = F(p) \text{ at } E = E_0\,.$$

The solution of problem (81), (82) for a flat capacitor ($x = 0$ — cathode, $x = d$ — anode, x — dimensional variable) assumes the form

$$\begin{aligned} q_0 &= q_*\left[F_0\,\frac{b_1+b_2}{b_1}\left(1 - \frac{b_1+b_2}{b_2}\,\frac{x}{d}\right) + \frac{n_c^2}{n_0^2}\,\frac{x}{d}\right] - e n_c\,,\\ q_* &= \frac{e^2 n_0^2 d}{\varepsilon\varepsilon_0 E_0}\,, \qquad E_0 = \frac{U}{d}\,, \end{aligned} \tag{83}$$

and in the case of a cylindrical capacitor ($r = R_1$ for a cathode, $r = R_2$ for an anode, r is the radial coordinate with the origin in the center of symmetry) one obtains

$$\begin{aligned} q_0 = q_*\Bigg[&\frac{b_1+b_2}{R_1^2 b_2}\left(\frac{b_2}{b_1}\int_r^{R_2} F_0 r\,\mathrm{d}r - \int_{R_1}^{r} F_0 r\,\mathrm{d}r\right)\\ &- \frac{n_c^2}{2n_0^2}\left(1 - \frac{r^2}{R_1^2}\right)\Bigg] - e n_c\,,\\ q_* = \frac{e^2 n_0^2 R_1}{\varepsilon\varepsilon_0 E_0}\,&, \end{aligned} \tag{84}$$

where $E_0 = U/(R_1 \ln h^{-1})$, and $h = R_1/R_2$.

Equations (83), (84) suggest that the predominance of impurity conduction, $n_0 \gg n_c$, is associated with the formation of a near-electrode volume charge with the sign opposite to electrode polarity (heterocharge). Such a distribution of the volume charge stabilizes the fluid; in other words, the electric field suppresses small velocity perturbations. In contrast, a homocharge forms near the electrodes undergoing intense injection, $n_c \gg n_0$, eventually leading to emerging instability of the equilibrium liquid state and the development of EHD flows.

6.3 Acoustic waves

The interplay between acoustic and ion waves is of importance for studying solution properties by the ultrasonic method [93]. For example, the frequency dependence of absorption coefficients is used to determine chemical reaction rate constants [44, 93]; the electric field induced by an ultrasonic wave contains information about ion masses [94] or micelle charges in a colloid solution [95].

Let us assume that acoustic probing occurs on a small time interval, such that injection charges have no effect on the bulk processes. Then, the bi-ion conduction model, in which dissociation of A^+B^- ion pairs yields free A^+ and B^- ions, is acceptable. Let us further assume that the acoustic oscillation period is much longer than the time τ_i of a charge random walk: $\omega^{-1} \ll \tau_i$, where ω is the acoustic wave frequency, and the inertia of ion motion can be neglected. Acoustic waves are considered against the background of a homogeneous quiescent state ρ_0, $\mathbf{V}_0 = 0$, T_0; in addition, $\mathbf{E}_0 = E_0\mathbf{e}_x$, and $n_{10} = n_{20} = n_0 = \sqrt{k_d N/\alpha_{11}}$, where coefficients k_d, α_{11} are taken at the T_0, E_0 values, with $\mathbf{e}_x$ being the unit vector in the direction of the x-axis along the electric field. Weak effects, such as the dielectrocaloric effect and $\varepsilon(T)$ dependence, are neglected.

Seeking a solution in the form of traveling waves $(\mathbf{V}, \rho, T, \Phi, n_i) \sim \exp[\mathrm{i}(\omega t - \mathbf{kr})]$, we obtain the following expression for the complex frequency [91]:

$$\omega^2 = a^2k^2 + \mathrm{i}\gamma\,, \qquad a^2 = c_s^2 + a_E^2\,,$$

$$a_E^2 = \rho_0\left(\frac{\varepsilon_\rho^2}{\varepsilon}\cos^2\theta - 0.5\rho_0\varepsilon_{\rho\rho}\right)\varepsilon_0 E_0^2\,,$$

where c_s and a are the isentropic and total speeds of sound, θ is the angle between the direction of plane wave propagation and the external field strength vector (the angle between $\mathbf{k}$ and $\mathbf{E}_0$), ε_ρ and $\varepsilon_{\rho\rho}$ are derivatives with respect to ρ, $\gamma = \gamma_0 + \gamma_{ch} + \gamma_J$ is the damping decrement defined by the sum of decrements of viscous (γ_0), Joule (γ_J), and chemical (γ_{ch}) dissipations. In other words, the damping coefficient $\alpha = \gamma/(2a\omega)$ consists of the above three terms.

The simple estimation suggests that the field effect on the speed of sound does not exceed fractions of a percent, even in strong enough fields ($E \sim 100$ kV cm^{-1}). Of special interest, in my opinion, is the influence of the field on the acoustic wave energy, attributable to the dissociation–recombination reaction:

$$\alpha_{ch} = c_v h_0\,\frac{c_s^2}{2a^3}\left(\frac{1}{c_v} - \frac{1}{c_p}\right)\left(\frac{\dot{\xi}_T}{\rho_0 c_v} - \frac{\varepsilon_\rho}{\varepsilon}\,\dot{\xi}_E E_0\cos^2\theta\right)\frac{\omega^2}{\omega^2 + 4\omega_e^2}\,,$$

$$\omega_e = 2\alpha_{11}n_0\,,$$

where h_0 is defined by formula (17). This suggests that if the wave propagates along the field ($\theta = 0$), the energy of strong enough electric fields, $\dot{\xi}_E E_0\varepsilon_\rho/\varepsilon > \dot{\xi}_T/(\rho_0 c_v)$, transfers into the acoustic wave energy, and the amplitude of this wave increases along the direction of its propagation and passes through a maximum in the high-frequency region ($\omega \gg \omega_e$). This effect occurs only in the strong-field region, where the dissociation of ion pairs by the electric field is especially pronounced. Strong pulsed fields are usually used to exclude Joule heating and breakdown in aqueous solutions and polar fluids [93].

7. EHD instability and development of EHD flows for symmetric electrodes

Flat, cylindrical, and spherical capacitors exemplify symmetric electrode systems. The hydrostatic equilibrium condition fulfilled in such systems is arrived at in the following way. From the momentum balance equation (2) at $\mathbf{V} = 0$, the equation $-\nabla p' + q\mathbf{E} = 0$ is derived. Applying the rot operation to this equation, we find that the equilibrium state is possible at $\nabla q \times \mathbf{E} = 0$, i.e., when vectors ∇q and $\mathbf{E}$ are collinear. Obviously, this condition is fulfilled in symmetric electrode systems. Next, as follows from Rayleigh's principle [88], the equilibrium state is stable when vectors ∇q and $\mathbf{E}$ ($\nabla q \uparrow\uparrow \mathbf{E}$) are unidirectional; when they are in the opposite direction ($\nabla q \uparrow\downarrow \mathbf{E}$), instability may develop. By way of example, it follows from formulas (83), (84) for flat and cylindrical capacitors in the inductionless approximation that instability emerges at a high enough level of injection:

$$n_c > n_0\sqrt{\frac{F_0(b_1 + b_2)^2}{b_1 b_2}}\,. \tag{85}$$

Of interest in EHD instability research is not only the fact of development of a flow in itself, but also the calculation of threshold voltages U_*, whose exceeding results in forming an EHD flow, and the detection of critical perturbations determining its structure. These observations provide an insight into mechanisms of fluid conductivity and information on the distribution of ionic components without direct (e.g., probing) measurements. It is in this order that these issues will be considered below.

7.1 EHD instability in a flat capacitor

Let us begin by considering EHD instability in a flat capacitor, where the inductionless approximation conditions are fulfilled:

$$C = \frac{d}{\xi_d} \ll 1\,, \qquad C_i = \sigma_c C = \frac{en_c d}{\varepsilon\varepsilon_0 E_0} \ll 1\,.$$

Calculations are made in dimensionless variables using the system of equations (69)–(72). In this case, equilibrium charge distributions are defined by the relations

$$n_{10} = Ca_1(1 - x)\,, \qquad n_{20} = Ca_2 x\,, \qquad n_{40} = 1 - C_i x\,,$$
$$a_1 = (1 + \beta_2)F_0\,, \qquad a_2 = \left(1 + \frac{1}{\beta_2}\right)F_0\,. \tag{86}$$

In what follows the solution is presented as the sum of equilibrium distributions and small perturbations, the dependences of which on time t and longitudinal coordinate y are determined by plane normal perturbations in

the form

$$\mathbf{V}(t,x,y) = \mathbf{u}(x)\exp(\lambda t - \mathrm{i}ky)\,,$$
$$n_j(t,x,y) = CN_j(x)\exp(\lambda t - \mathrm{i}ky)\,, \qquad j = 1,2\,,$$
$$n_4(t,x,y) = C_{\mathrm{i}}N_j(x)\exp(\lambda t - \mathrm{i}ky)\,,$$
$$\tilde{p}(t,x,y) = P(x)\exp(\lambda t - \mathrm{i}ky)\,.$$

For small-perturbation amplitudes, the following problem is staged:

$$\lambda\mathbf{u} = -\left(\mathbf{e}_x\frac{\mathrm{d}}{\mathrm{d}x} - \mathrm{i}k\mathbf{e}_y\right)P + R_{\mathrm{e}}^{-1}\hat{L}\mathbf{u} - CMq\mathbf{e}_x\,, \qquad \operatorname{div}\mathbf{u} = 0\,, \tag{87}$$

$$\lambda N_1 - \beta_1\frac{\mathrm{d}N_1}{\mathrm{d}x} = -a_1u_x\,, \qquad \lambda N_2 + \frac{\mathrm{d}N_2}{\mathrm{d}x} = -a_2u_x\,, \tag{88}$$
$$\lambda N_4 + \beta_4\frac{\mathrm{d}N_4}{\mathrm{d}x} = u_x;$$
$$q = C(N_1 - N_2) - \sigma_{\mathrm{c}}C_{\mathrm{i}}N_4\,, \qquad \hat{L} \equiv \frac{\mathrm{d}^2}{\mathrm{d}x^2} - k^2\,,$$

with boundary conditions

$$x = 0\colon\ \mathbf{u} = 0\,,\ N_2 = N_4 = 0; \quad x = 1\colon\ \mathbf{u} = 0\,,\ N_1 = 0\,. \tag{89}$$

System (87)–(89) represents the boundary problem for the eigenvalues of λ. Since the problem is not self-conjugate, the spectrum of λ may be either real-valued (monotonic perturbations) or complex (vibrational perturbations). Experimental studies [4, 23, 92] showed that isothermal EHD instability normally develops in the presence of monotonic perturbations. Then, the critical voltage U_* is found from the condition $\lambda = 0$. After a few transformations, the following spectral problem with respect to parameter B is obtained from Eqns (35)–(37):

$$\hat{L}^2u = k^2B\left(\int_0^x u\,\mathrm{d}x - a\int_x^1 u\,\mathrm{d}x\right), \qquad u = u_x\,;$$
$$x = 0\,, \quad x = 1\colon \quad u = \frac{\mathrm{d}u}{\mathrm{d}x} = 0; \tag{90}$$
$$B = R_{\mathrm{e}}C^2M\left(\frac{\sigma_{\mathrm{c}}^2}{\beta_4} - a_2\right), \qquad a = \frac{a_1}{\beta_1(\sigma_{\mathrm{c}}^2/\beta_4 - a_2)}\,.$$

It can be seen using explicit expressions for dimensionless parameters [see formulas (69)–(72)] that monotonic EHD instability will develop only in the injection conduction mode, when $\sigma_{\mathrm{c}}^2 > \beta_4a_2$, in agreement with condition (85). The Bubnov–Galerkin method was applied to numerically solve problem (90) by expanding the solutions in basis functions $u_n = x^n(1-x)^2$ [96]. Parameter a was fixed and wave number k varied so that function $B(k)$ acquired a minimal value. The results of the calculation of minimal $B_*(k_*)$ values and the corresponding k_* at several a are listed in Table 2.

Table 2

a	0	0.1	0.2
k_*	4.5	4.3	3.8
B_*	221	270	374

The value of $a = 0$ corresponds to the case of unipolar ion injection, with its growth reflecting the enhancement of impurity conduction. It follows from the above data that a rise in impurity conductivity leads to an increase in the critical perturbation wavelength $l_* = 2\pi d/k_*$, so that equalization of impurity and injection conductivities, when $a \to \infty$, results in $k_* \to 0$, $l_* \to \infty$, i.e., electroconvective (EC) cells are smeared over the entire interelectrode space. The shape of the EC cells is conveniently described by the ratio of their side lengths, $d : (l_*/2) = k_*/\pi$. Numerical data indicate that in the course of unipolar injection the EC cells are elongated in a transverse direction ($d : (l_*/2) = 1.4$) (Fig. 11a); they become stretched longitudinally with the growth in impurity conduction (Fig. 11b).

Increased impurity conductivity is responsible not only for a change in EC cell geometry, but also for the rise in the critical value of threshold voltages U_*. Therefore, the impurity conduction essentially hampers the observation of isothermal electroconvection in a flat capacitor. A stable EC motion in the flat capacitor is observed during unipolar injection from ionite membranes into polar liquids, such as nitrobenzene or pyroline [32, 33]. It should be noted that flat perturbations are unstable, as in the case of thermal instability in the gravitational field, and EC cells acquire a hexagonal shape resembling Benard cells (Fig. 11c).

For weak unipolar injection ($C_{\mathrm{i}} \ll 1$), the injection law can be determined from the threshold voltage U_* at the electrodes. Then, $B_* = R_{\mathrm{e}}C^2M\sigma_{\mathrm{c}}^2/\beta_4 = 221$ and one arrives at

$$B_* = \frac{e^2d^3}{\varepsilon\varepsilon_0b_4\eta}\,\frac{n_{\mathrm{c}}^2(E_*)}{E_*} = 221\,, \qquad E_* = \frac{U_*}{d}\,. \tag{91}$$

Relation (91) constitutes an equation in U_*. Because function $n_{\mathrm{c}}(E_*)$ does not show an explicit dependence on d, this relation can be used in determining the injection law by measuring E_* at various d. Certainly, the experimental realization of this method requires high-quality measurements and the employment of precision instruments.

Relation (91) leads to an important conclusion regarding the so-called autonomous injection level, on which calcula-

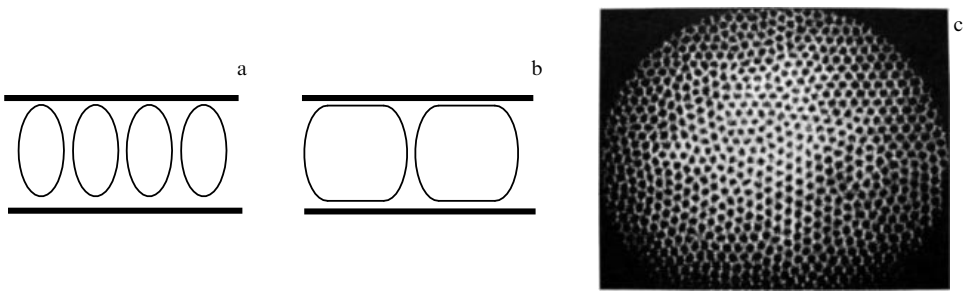

Figure 11. The shapes of EC cells: (a) for unipolar injection, and (b) for injection and impurity conductivity; (c) shadow picture of EC cells in a flat capacitor for unipolar injection in pyraline-1460 [23]. Interelectrode gap measures 0.6 mm, and $U = 60$ V.

tions were based [4, 23]. If $n_c = \text{const}$, it follows from formula (91) that condition $B < B_*$ is fulfilled for $U > U_*$, implying the absence of electroconvection, contrary to available experimental data. We believe that the postulate of injection autonomy needs to be more thoroughly substantiated; as it is, it is incorrect to apply this hypothesis in calculations.

To conclude, we note that in the case of high-level injection ($C_i \gg 1$), the stability criterion can be written out in the form [4, 23]

$$T_* = \frac{U_*}{U_0} = 161\,, \qquad U_0 = \frac{\eta b}{\varepsilon\varepsilon_0}\,, \tag{92}$$

where b is the mobility of the ions being injected.

Relations (92) indicate that the threshold field strength at a high injection level depends neither on the injection law nor on the electrode spacing d. The independence from d has been reported in many experiments [4, 23, 71, 92]. However, caution is needed when applying relations (92) to the explanation of this effect, because the instantaneous switching-on of high voltage may trigger an EHD flow due to d-independent instability of the ion cloud front (see Section 6).

7.2 EHD instability in a cylindrical capacitor

EHD instability in a cylindrical capacitor is interesting first and foremost due to electroconvection, readily apparent even at weak injection and the presence of impurity conduction. The stability of EHD flows can be accounted for by a markedly enhanced field strength on the electrode surface for small radii of the central electrode. This eventually leads to the dominance of injection conduction, and thereby maintains flow stability.

In the present case, flat perturbations correspond to dependences $f(t, r, \varphi) = f(r)\exp(\lambda t - in\varphi)$, where r, φ are the radial and angular coordinates of the cylindrical system of coordinates, $n = 1, 2, 3, \ldots$. Calculations analogous to those for a flat capacitor indicate that in the inductionless approximation the critical voltage is specified by the following spectral problem with respect to parameter B:

$$\hat{L}^2 u = n^2 B\left(\int_1^s us\,\mathrm{d}s - \alpha_1\int_s^H F_0 us\,\mathrm{d}s - \alpha_2\int_1^s F_0 us\,\mathrm{d}s\right); \tag{93}$$

$$s = 1, \quad s = \frac{1}{h} = \frac{R_2}{R_1}: \quad u = \frac{\mathrm{d}u}{\mathrm{d}s} = 0;$$

$$\hat{L} = \frac{1}{s}\frac{\mathrm{d}}{\mathrm{d}s}\left(s\frac{\mathrm{d}}{\mathrm{d}s}\right) - \frac{n^2}{s^2}\,, \qquad s = \frac{r}{R_1}\,, \qquad u = su_r\,,$$

$$B = R_e C^2 M\,\frac{\sigma_c^2}{\beta_4}\,, \qquad \alpha_1 = \frac{a_1\beta_4}{\beta_1\sigma_c^2}\,, \qquad \alpha_2 = \frac{a_2\beta_4}{\sigma_c^2}\,,$$

where the dimensionless parameters have the same sense as in the set of equations (69)–(72) at $R_1 = d$, and $E_0 = U/(R_1 \ln h^{-1})$.

Problem (93) was solved by the Bubnov–Galerkin method [96], and the calculation accuracy was verified by another method, i.e. the transformation of the differential equation into an integral one, with its minimal eigenvalue found by iterations according to algorithm described in Ref. [65]. The results of computations of $B_* = B(n_*)$, where n_* is the value of n at which $B(n)$ is minimal, are presented in Table 3 for different ratios of electrode radii, $h = R_1/R_2$, under conditions of unipolar injection from the central electrode.

Table 3

h	0.05	0.1	0.2	0.3	0.4	0.5
B_*	0.00496	0.0825	1.55	10.1	44.7	617
n_*	2	3	3	4	5	7

The critical field strength at the central electrode, E_*, or the voltage at electrodes, U_*, are given by the relations

$$B_*(h) = \frac{e^2 R_1^3}{\varepsilon\varepsilon_0 b_4 \eta}\,\frac{n_c^2(E_*)}{E_*}\,, \qquad E_* = \frac{U_*}{R_1 \ln h^{-1}}\,, \tag{94}$$

where the value of $B_*(h)$ ensues from the above numerical data.

It follows from the data presented that the number of EC cells equals 4 at a small electrode radii ratio, $h \leqslant 0.05$; as h increases, two more cells appear successively. These conclusions are in excellent agreement with the experimental data on electroconvection in technical grade transformer oil having conductivity $\approx 10^{-13}\,\Omega^{-1}\,\mathrm{cm}^{-1}$ [97] (Fig. 12). Measured VACs and threshold voltage measurements [98] suggest that electroconvection develops in a mixed dissociation–injection conduction mode, with the electric field-induced increase in dissociation playing an important role. This accounts for the discrepancy between experimentally found threshold voltages and theoretical estimates based on formula (94), from which it is possible to determine the injection law, i.e., the functional dependence $n_c(E)$, in a wider range of field strengths than in a flat capacitor. Relations (94) were utilized in calculating critical parameters for arbitrary-level unipolar injection from the central electrode [96], assuming the linear injection law $n_c(E) = \eta_c E$. In this case, instability was characterized by

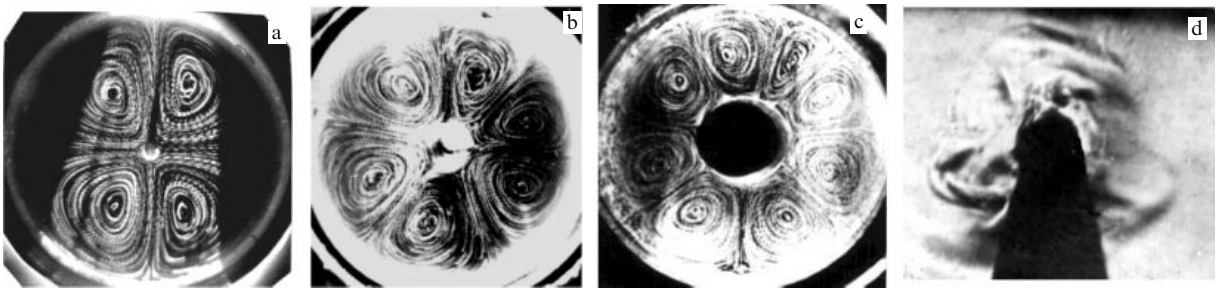

Figure 12. EHD flow streamlines of transformer oil in a cylindrical capacitor [97]. Stationary patterns of streamlines at different diameters R_1 of the inner electrode: (a) $h = 0.027$, $R_1 = 0.025$ cm; (b) $h = 0.09$, $R_1 = 0.1$ cm; (c) $h = 0.15$, $R_1 = 0.25$ cm. The number of EHD cells grows, remaining even, as R_1 increases. (d) The shadow picture of an EHD flow.

Table 4

h \ C_i	0.1	1	10	20	100
0.1	0.88(2)	35.6(3)	30.3×10^2(3)	30.1×20^2(3)	30×10^4(3)
0.2	4.48(3)	75.4(3)	57.2×10^2(3)	56.21×20^2(3)	54×10^4(4)
0.3	17.28(4)	167.2(4)	91.4×10^2(4)	88×20^2(4)	85×10^4(5)
0.5	212(7)	763(7)	222×10^2(7)	200×20^2(7)	185×10^4(8)

three parameters

$$C_i = \frac{e\eta_c R_1}{\varepsilon\varepsilon_0}, \qquad B = \frac{e^2 R_1^3}{\varepsilon\varepsilon_0 b\eta}\,\frac{n_c^2(E_0)}{E_0}, \qquad E_0 = \frac{U}{R_1 \ln h^{-1}}.$$

The results of calculating $B_* = B(n_*, h)$ for various injection levels C_i and different h are collated in Table 4 (values in round brackets correspond to n_*).

These numerical data suggest asymptotics $B = TC_i^2$, where $T = U/U_0$, $U_0 = \eta b/(\varepsilon\varepsilon_0 \ln h^{-1})$, at high injection levels ($C_i \gg 1$). In other words, the threshold voltage does not depend on the injection law, as in the flat capacitor case, but does depend on the electrode radii ratio.

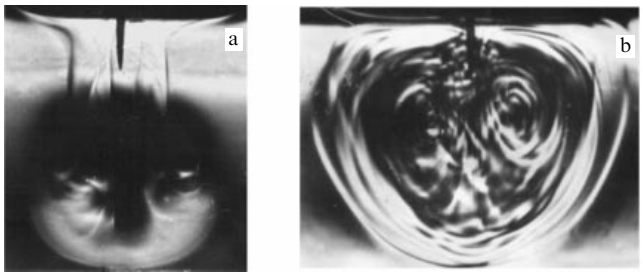

Figure 13. Shadow pictures of EHD flows in a needle–plane system [92]: (a) EHD flow upon switching on the high-voltage field, and (b) fully-developed EHD flow.

8. Asymmetric electrode systems

In needle–plane, blade–plane, and other types of asymmetric electrode systems, the equilibrium condition $\nabla q \times \mathbf{E} = 0$ is not fulfilled. Nevertheless, the threshold nature of the development of EHD flows persists [12, 13]. This fact has for a long time remained enigmatic. However, the use of an approach based on the dissociation–injection model [53] showed that this phenomenon is attributable to the substitution of the injection conduction mode for the dissociation one. Due to this, EHD flows for asymmetric electrodes, as a rule, develop in a mixed dissociation–injection conduction mode, especially at the initial stages, making their study somewhat difficult due to both the robustness of the system of equations and particularly their nonlinearity.

The main patterns of EHD flows in the system of asymmetric electrodes are considered below based on concrete examples with the employment of both the analytical and numerical methods. The choice of a particular model will be based on available experimental data.

8.1 Peculiarities of EHD flows for asymmetric electrodes

Efficacious visualization of EHD flows is performed with the aid of air bubbles blown out of a polyvinyl chloride tube ≈ 50 μm in diameter [13] and a stroboscopic illumination system; the bubble velocity — and therefore the rate of fluid movement — is evaluated from the track length. Notice that the bubbles do not conduct electric current and have a small virtual mass; therefore, their influence on the EHD flow should be negligible. However, they can acquire a charge, which suggests the possibility of initiating EHD movements by bubbles or disperse particles. To this effect, experiments on the fixation of EHD flows were carried out by the shadow method [92].

The results of research in a needle–plane electrode system are presented in Fig. 13, showing that EHD motion develops in the absence of bubbles, too; in other words, charge injection from the needle takes place. The EHD movements were detected both at the initial stage immediately after the high voltage was instantaneously switched on (Fig. 13a) and at the stage of well-developed motion (Fig. 13b). Figure 13a shows that at the onset of an EHD flow the charge is injected from the entire needle surface, and not only in the vicinity of its tip, where the electric field strength has a maximum value. The presence of the bulk charge contributes to the charging of the bubbles and the formation of their characteristic helical tracks.

8.2 EHD flows in a plane-curved electrode system

Unlike the universally accepted notion of 'dissociation conduction', the notion of ion injection from electrodes has a much shorter history and has not yet provided a popular method for studying EHD phenomena. A characteristic example of EHD flows associated with dissociation–injection conduction is cellular electroconvection in a plane–curved electrode system [80, 98] (Fig. 14). The existence of ion injection was proved as described below [80]. The transformer oil was purified by passing it through glass filters to reach a conductivity of $10^{-14}\ \Omega^{-1}\ \mathrm{cm}^{-1}$, and supplemented with iodine (I_2) to obtain a solution conductivity of $10^{-12}\ \Omega^{-1}\ \mathrm{cm}^{-1}$. The solution was added into a cell with plane and curved electrodes. Given that the bent electrode is negative, the flow rate is high, while the change in polarity causes electroconvection to damp. A similar dependence holds for the current. These features are attributable to the injection of negative charges from the cathode as a result of occurring the reduction electrochemical reaction involving iodine. Relevant calculations are consistent with experimental evidences [80]. Here are the results of calculations for different limiting cases.

Let us choose a system of coordinates, as shown in Fig. 14b. The equation for the curved electrode is taken in the form $y(x) = d + a\cos(\Omega x)$, where Ω denotes the degree of bending, and a is the amplitude. Analytical computations are possible in a linear approximation for a small electrode bending amplitude $\xi = a/d \ll 1$ in the inductionless approximation ($C \ll 1$, $C_i \ll 1$). There are two expressions for the longitudinal velocity component V_y and they are presented below.

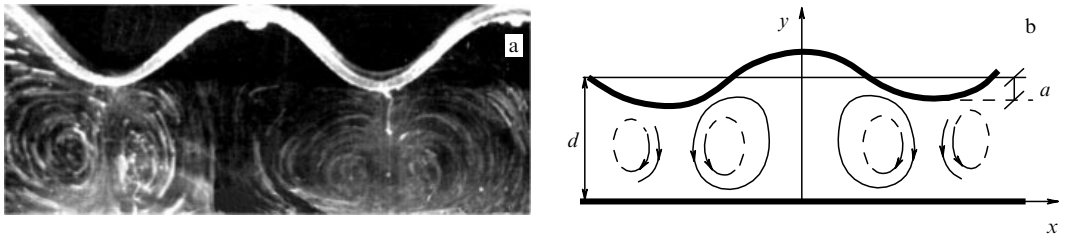

Figure 14. (a) Electroconvection in a plane–curved electrode system [80]; the curved electrode is negative, interelectrode gap ≈ 2 cm, and voltage is 5 kV. (b) The choice of the coordinate system.

In the case of ion injection from a strongly bent electrode with $\omega = \Omega d \gg 1$, in its neighborhood $y \sim d$ one finds

$$V_1 \equiv V_y = \frac{ed^2E_0}{\eta}\,\frac{\xi}{\omega^2} \times \left[-n_0C\left(1+\frac{1}{\beta_2}\right)(2F - F_E'E_0) + \omega\,\frac{\mathrm{d}n_\mathrm{c}}{\mathrm{d}E_0}\,E_0\right]\cos(\Omega x)\,, \qquad F = F(E_0)\,, \quad F_0' = \frac{\mathrm{d}F}{\mathrm{d}E_0}\,, \quad n_\mathrm{c} = n_\mathrm{c}(E_0)\,. \tag{95}$$

For unipolar conduction and ion injection from the plane electrode ($y = 0$), one obtains

$$V_2 \equiv V_y = \frac{ed^2E_0^2}{\eta}\,\frac{\mathrm{d}n_\mathrm{c}(E_0)}{\mathrm{d}E_0}\,\frac{\exp(-\omega)}{\omega} \times \left[1 - \left(1+\omega\,\frac{y}{d}\right)\exp\left(-\omega\,\frac{y}{d}\right)\right]\cos(\Omega x)\,. \tag{96}$$

Hence, we reach the following conclusions.

(1) In a weak field region with a predominance of impurity conduction, $2F > F_E'E_0$, $2n_0C(1+1/\beta_2)F > \omega(\mathrm{d}n_\mathrm{c}/\mathrm{d}E_0)E_0$, the fluid flows toward surface convexities of the curved electrode, with the flow rate being field-independent if $C \ll 1$. As the field strength increases ($F_E'E_0 > 2F$) and injection remains weak, the flow reverses direction and travels away from the convexities. The flow rate then grows exponentially with the field strength.

(2) At a high enough ion injection level from the curved electrode, viz. $\omega(\mathrm{d}n_\mathrm{c}/\mathrm{d}E_0)E_0 > n_0C(1+1/\beta_2)\times|2F - F_E'E_0|$, the fluid flows from its convexities with a rate determined by the injection law. For example, the flow rate in the case of linear injection, $n_\mathrm{c} = \eta_\mathrm{c}E$, is quadratic in field strength:

$$V_y = \frac{ed^2}{\eta}\,\frac{\xi}{\omega}\,\eta_\mathrm{c}E_0^2\cos(\Omega x)\,. \tag{97}$$

(3) In strong enough electric fields, when injection conduction predominates, the flow rate during injection from the plane electrode is much lower than the electroconvection rate under ion injection from the curved electrode: $V_1 \gg V_2$, as confirmed in experiments on EHD flows in iodine-containing transformer oil solutions with immersed copper electrodes [80].

The results of calculations [99] indicate that the above features are common to all asymmetric electrode systems. For example, in weak-field regions and, consequently, low-level ion injection from tapered electrodes (needles, blades, etc.), the fluid travels toward their sharpened edges, i.e., to the field concentration region. This fact is accounted for by the formation of a heterocharge near the edges where the Coulomb force is directed to the electrode. Numerical calculations demonstrate that such flows are especially slow. A change of the conduction mode resulting in the predominance of the ions being injected initiates formation of a homocharge near the tips. Then, the Coulomb force is directed away from the tip and the flow becomes reversed. Such flows are so rapid that they can be seen with the naked eye, giving an impression of the threshold character of flow development in asymmetric electrode systems.

8.3 Numerical analysis of EHD flows

Let us consider a blade–plane electrode system (Fig. 15). Clearly, the ion injection process dominates at the tapered electrode due to the extremely high field strength at its sharp end. Therefore, the electroconvection in the blade–plane electrode system can be described in terms of a three-ion model in dimensionless variables, i.e., using steady-state equations (69)–(72).

It can be assumed without loss of generality that the tapered electrode places the part of the cathode. Due to the essential nonlinearity of the equations and complicated

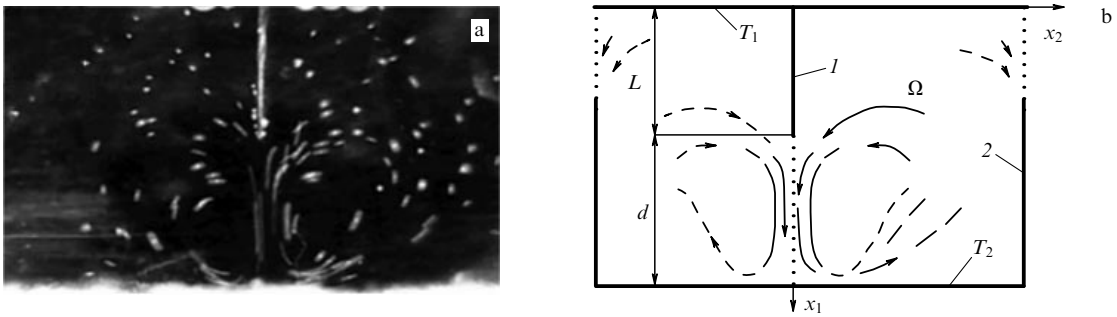

Figure 15. Electroconvection in a blade–plane electrode system. (a) Photograph of flow streamlines: interelectrode gap is 1.5 cm, and voltage $U = 10$ kV. (b) Computational domain geometry in numerical simulation in the form of a rectangle Ω shaped by electrodes *1* (cathode) and *2* (anode) (solid lines) and symmetry lines (straight dotted lines); T_1 (T_2) is the top (bottom) electrode temperature.

geometry of the flow region, the comprehensively formulated problem can only be investigated by numerical methods. With this in mind, we shall formulate a more complete system of boundary conditions for ionic components, taking into account injection of impurity ions due to the participation of ion pairs in electrochemical reactions at the electrodes, as well as the finiteness of the ion discharging rate.

As shown in experiments [13], EHD flows in tapered electrode systems can also develop in a strong enough electric field in the absence of special activating additions like iodine, butyl alcohol and some others. This effect may be due to minor admixtures of water, dissolved oxygen, or other substances. Therefore, impurity ions can also be injected from electrodes as a result of electrochemical reactions. Their formation rate can be described by injection functions $n_A(E)$ for A^+ ions, and $n_B(E)$ for B^- ions. Ion injection is accompanied by discharging of ions with opposite polarity (counterions) at the electrodes. At a finite discharging rate, the counterions accumulate in near-surface diffusion layers as thick as [25]

$$\xi_D = \frac{\varphi_0}{E_v}\,, \tag{98}$$

where $\varphi_0 = k_B T/e$, E_v is the electric field strength at the DEL–liquid interface. Accumulation of counterions at the electrodes gives rise to two important effects: (1) reduction in ion injection due to the altered catalytic activity of the surface, and (2) shielding of an external field leading to a fall in the external field strength in the bulky liquid, and thereby to the decay of electroconvection. Field strength E_v at the DEL border and local strength E_{loc} on the surface are related by the expression $E_v = \beta_D E_{loc}$, where β_D is the amplification coefficient by the double electrical layer [25]. Shielding of the external field by the DEL field can be specified in the boundary conditions by a voltage drop at the electrode:

$$\Delta U = \int_{r_0}^{\xi_D} E\,\mathrm{d}x \approx (E_{loc} - E_v)\xi_D = (\beta_D - 1)E_v\,, \tag{99}$$

where r_0 is the effective ion size.

The boundary conditions for counterions are given by the relationship between charge concentrations at the electrode, $n_i = n_i(r_0)$, and at the DEL border, n_{iv} [25]:

$$n_i = K_r n_{iv}\,, \qquad K_r = \frac{b_i E_v}{k_r}\,, \tag{100}$$

where k_r is the counterion discharging rate constant.

It follows from formula (100) that there are no ions discharging on the electrodes at high discharging rates (instantaneous discharging), $K_r \ll 1$. In this case, $\beta_D = 1$ [25] and there is no voltage drop at the electrode.

Thus, the boundary conditions for dimensionless variables take the form

at the anode:

$$V = 0\,, \quad \Phi = 1\,, \quad n_1 = \frac{n_A(E)}{n_0} \equiv f_A(E)\,, \tag{101}$$

at the cathode:

$$V = 0\,, \quad \Phi = 0\,, \quad n_2 = \frac{n_B(E)}{n_0} \equiv f_B(E)\,, \quad n_4 = \frac{n_c(E)}{n_c(E_0)} \equiv f_c(E).$$

The numerical solution to problem (69)–(72), (101) was sought in a plane formulation in accordance with the algorithm proposed in Ref. [100] and modified in paper [99]. The computational domain geometry was chosen with account of the system's symmetry, as illustrated in Fig. 15b. Such a choice of the electrode system is convenient in that, first, it widens discharging surface *2* of the ion collector and, second, it permits considering two processes in a single calculation, namely EHD flows during injection from cathode *1* and in the absence of injection from anode *2* whose neighborhood is dominated by dissociation conduction. The hydraulic medium was an iodine-containing transformer oil solution in which intense injection of negative ions occurred from the cathode at relatively low voltages. Calculations demonstrated that matching of volt–ampere and hydrodynamic characteristics is feasible only for the linear injection law, i.e., at $f_c(E) = E$ in formula (101), and low mobility of ions being injected. This inference is consistent with the conclusion that the ions being injected in a saturated iodine solution are clusters with effective radii on the order of 120 nm [24], whose mobility is substantially lower than that of monoions. Taking together all these facts and bearing in mind a closeness in the mobilities of positive and negative impurity monoions [19, 24], the following parameters were used in calculations: $\rho = 1$ g cm^{-3}, $b_4 = 0.2b_1$, $b_1 = b_2 = 10^{-8}$ m^2 V^{-1} s^{-1}, $\sigma = 10^{-11}$ Ω^{-1} m^{-1}, $\varepsilon = 2.1$, $\eta = 0.2$ P, $\lambda = 0.119$ W m^{-1} K^{-1}, and $c_p = 2 \times 10^3$ J kg^{-1} K^{-1}. For the linear injection law, the dimensionless parameters are convenient to write down in the form

$$C_i = \frac{e\eta_c d}{\varepsilon\varepsilon_0}\,, \quad \sigma_c = C_i S_c R_e\,, \quad S_c = (1 + \beta_2)S\,, \quad S = \frac{\varepsilon\varepsilon_0 v}{\sigma_0 d^2}\,.$$

Parameter C_i defines the injection level of X^- ions, while S and R_e specify the influence of impurity conduction and voltage at the electrodes, respectively. The value of the injection coefficient was found from the relations $en_c(E_*)\mu_4 E_* = j_*$ and $n_c(E_*) = \eta_c E_*$, where $e\eta_c = 2.4 \times 10^{-9}$ A s V^{-1} m^{-2} for the pure transformer oil dried for 4 days (based on the experimental VAC in a flat capacitor at $E = 10$ kV cm^{-1}). Numerical calculations were carried out at $d = 1$ cm at different voltages, from $U = 2$ kV (onset of intense EHD flow) to $U = 15$ kV (fully developed EHD flow). Here are typical values of dimensionless parameters for pure transformer oil: $C_i = 1.1$, $S = 0.37$, $M = 185$, and $R_e = 5$ ($U = 10$ kV). All observations and conclusions concerning electroconvection in the plane–periodically curved electrode system were confirmed by our calculations (see Section 4.2).

The development pattern of electroconvection in a weak-field region is illustrated in Fig. 16. Calculations showed that for $U \leqslant 1$ kV, i.e., at weak injection, the flow is directed to the tapered edges of the electrodes, but the flow rate is extremely low (below 1 mm s^{-1}). At $U \sim 2$ kV, a small vortex forms near the injector electrode (Fig. 16a), which rapidly grows as the field strength increases and spreads over the entire region between the injector electrode and the counterelectrode (Fig. 16b). Near the sharpened tip where injection is absent, the flow retains its direction to the tip. Calculations gave evidence that matching theoretical and experimental data [13] by streamlines and flow rate along the symmetry axis from the injector electrode (central jet) takes place only for high-level injection and low mobility of the ions being injected. Independent experimental measurements of flow rate distributions in dried transformer oil made by A E Kuz'ko (Fig. 17a) are also in qualitative agreement with our calculations (Fig. 17b). For example, the jet length l is related

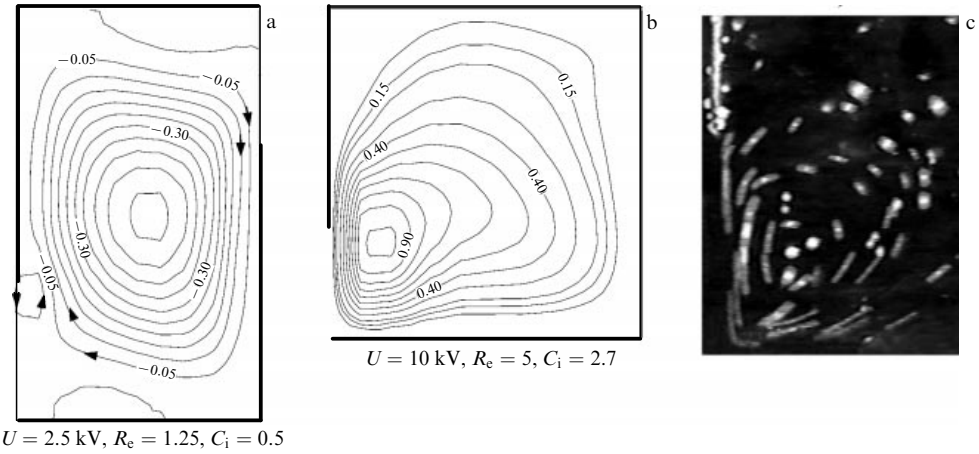

Figure 16. (a) Theoretical streamlines during weak unipolar injection of X^- ions from the cathode in the absence of impurity ion injection in iodine-containing transformer oil and instantaneous ion discharging; (b) fully developed flow; (c) a snapshot of EHD flow (exposure 0.04 s), voltage $U = 10$ kV, and interelectrode gap 1 cm.

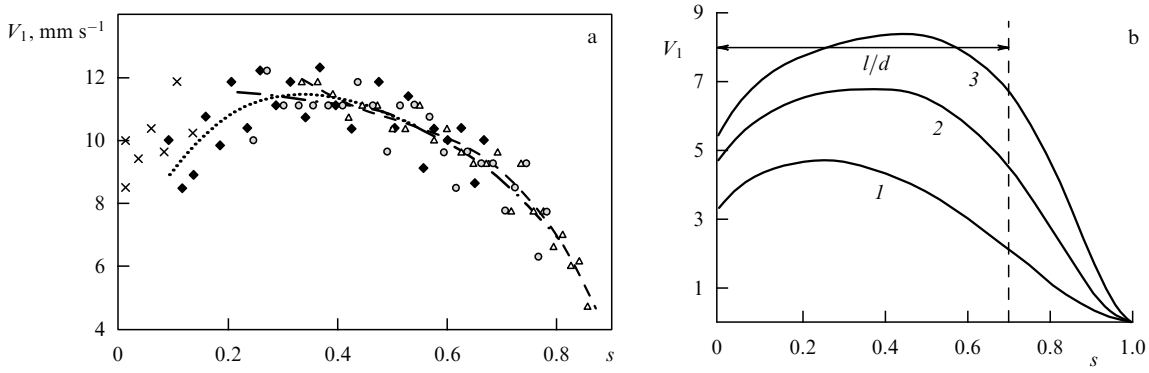

Figure 17. (a) Experimental dependence of the flow rate V_1 along the jet axis at $d = 1.5$ cm, and $U = 5$ kV. (b) Results of calculations of the longitudinal dimensionless flow rate component along the symmetry axis [coordinates $s = (x_1 - L)/d$ (Fig. 15b)] from the injector electrode (central jet) for the strong injection case, $C_i = 2.7$: *1* — $U = 5$ kV, *2* — $U = 10$ kV, and *3* — $U = 15$ kV. Instantaneous ion discharging.

to the distance d as $l \approx 0.7d$. The flow rates are of the same order of magnitude, too; in particular, in the central jet for weak and strong injections at $U = 5$ kV, they are $V_1 = 1.5$ cm s^{-1} and 5 cm s^{-1}, respectively, consistent with theoretical results (Fig. 17b). However, a more thorough evaluation of injection parameters and ion discharging coefficients is needed to reach complete quantitative agreement. It was shown by calculation that the EHD flow rate V_1 drops appreciably at the finite ion discharging rate, e.g., by 30% at $K_r \sim 3$ and $U = 5$ kV.

The following conclusions can be drawn from the results of calculations:

(1) In the absence of ion injection (dissociation conduction mode), the fluid travels to the blade edge at a very low rate (less than 1 mm s^{-1}). At a high enough voltage, when injection conduction begins to dominate, the fluid flows away from the injector electrode (see Fig. 16), and the flow rate amounts to 10 cm s^{-1}. This effect accounts for the apparent threshold nature of the flow development in an asymmetric electrode system.

(2) The linear injection law agrees with both the flow field and VAC.

(3) Experimental and theoretical streamlines coincide when the mobility of the ions being injected is lower than the monoion mobility.

(4) The EHD flow rate decreases at a finite ion discharging rate.

(5) Studies into the EHD flow structure and flow field distribution coupled with VAC analysis permit elucidating mechanisms of ion injection from electrodes.

8.4 EHD heat exchange

The enhancement of heat transfer from a heated electrode due to the formation of boundary EHD layers is a very important application of EHD flows. In engineering practice, heat transport is characterized by heat exchange coefficient α, defined as $\dot{Q} = \alpha \Delta T$, where $\dot{Q}$ is the heat flux from the entire surface per unit time, and $\Delta T = T_2 - T_1$ is the temperature difference ($T_2 > T_1$). In the Boussinesq approximation, the temperature field distribution in dimensionless variables ($\theta = (T - T_1)/\Delta T$) is written out as

$$\mathrm{Pr}\, R_e \mathbf{V} \nabla \theta = \Delta \theta \,, \tag{102}$$

where $\mathrm{Pr} = \nu/\kappa$ is the Prandtl number (κ is the thermal diffusivity). Assuming the bottom electrode to be hot (Fig. 15b) and disregarding heat transfer through thin blades, the boundary conditions can be written in the following form:

$$\begin{aligned} &\text{top electrode } (x_1 = 0): \quad \theta = 0; \\ &\text{bottom electrode } (x_1 = L_1): \quad \theta = 1; \\ &\text{symmetry lines } (x_2 = 0,\ x_1 = L_2): \quad \frac{\partial \theta}{\partial x_2} = 0 \,. \end{aligned} \tag{103}$$

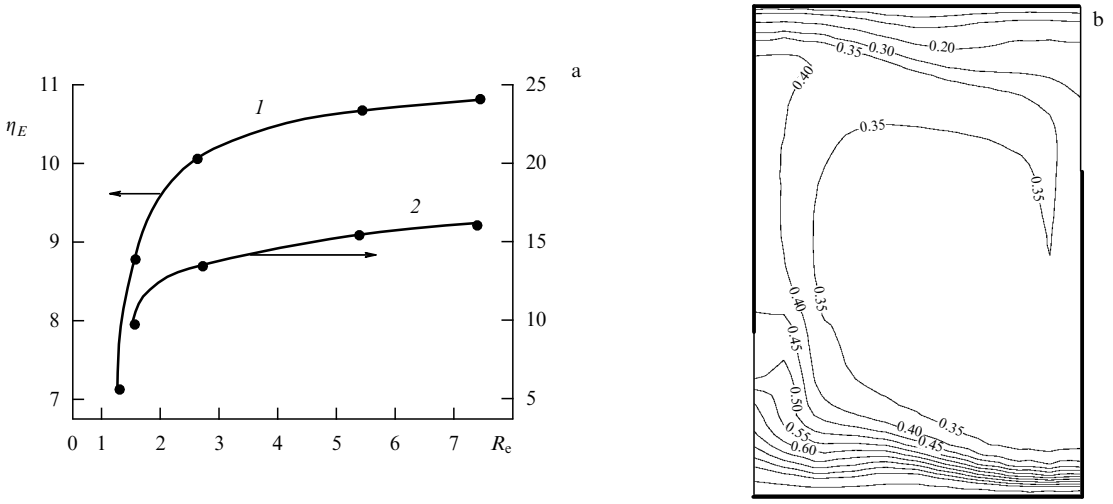

Figure 18. (a) EHD heat transfer coefficient plotted vs applied voltage (instantaneous ion discharging): *1* — weak injection, $C_i = 0.5$; *2* — strong injection, $C_i = 2.7$. (b) Isotherms at $C_i = 0.5$ and $R_e = 1.25$.

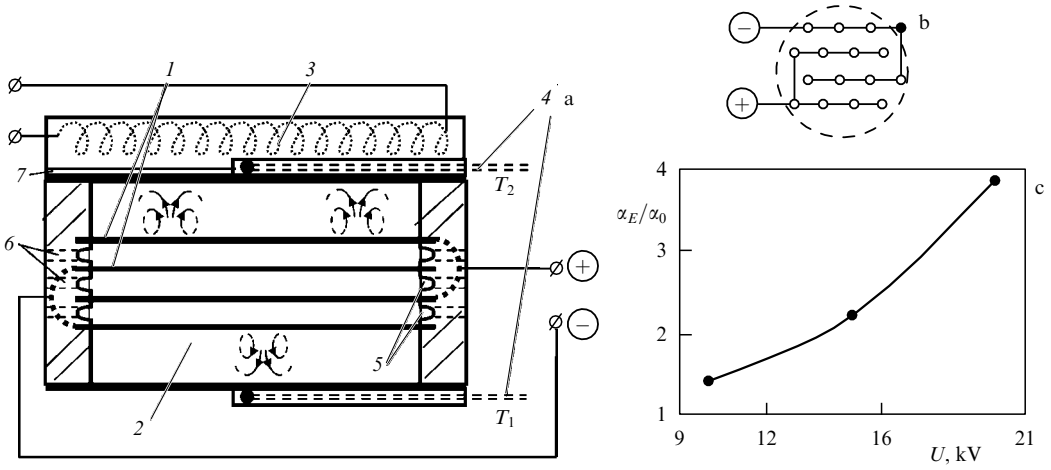

Figure 19. (a) Schematic of a wire EHD heat exchanger: *1* — wire electrodes, *2* — fluid, *3* — heater coil, *4* — thermocouple leads, *5* — interelectrode recesses, *6* — flushing channels, *7* — mica plate. (b) Arrangement of electrodes. (c) Measurement results [56].

Let us find the heat transfer amplification coefficient as the ratio of the thermal flux $\dot{Q}_E = \alpha_E \Delta T$, $\alpha_E = \lambda \int_0^{L_2} \partial\theta/\partial x_1 \, dx_2$ in an electric field calculated at the bottom electrode to the thermal flux $\dot{Q}_0 = \alpha_0 \Delta T$, $\alpha_0 = \lambda(L_2/L_1)$ in a quiescent fluid: $\eta_E = \dot{Q}_E/\dot{Q}_0$. The results of calculations of coefficient η_E presented in Fig. 18a suggest that heat transfer is effectively enhanced by an electric field at instantaneous ion discharging: $\eta_E \sim 10$ and $\eta_E \sim 20$ for weak and strong injections, respectively. The analysis of isotherms (Fig. 18b) shows that heat transfer largely occurs through boundary layers, and the fluid temperature at the interface between them is roughly constant. In experiments, a system of wire electrodes arranged in a chess-board fashion is usually utilized to enlarge the injecting surface area and prevent a breakdown [56, 101] (Fig. 19). The measured heat transfer amplification coefficient is relatively small; it does not exceed $\eta_E \approx 4$ at rather high voltages ($U \approx 20$ kV). Such small η_E values appear to be due to the finiteness of the ion discharging rate, which poses an important problem of identifying a buffer charge carrier from the injector to the ion collector, i.e., searching for an admixture readily ionized on the injector and rapidly discharged back into the original neutral material on the collector.

9. Conclusion

Today, electrohydrodynamics has established itself as a self-contained, rapidly developing scientific discipline. Scientific conferences are held on a regular basis in Russia (Saint Petersburg State University and P G Demidov Yaroslavl' State University), Europe, South-East Asia, and the USA. It is universally accepted that ionic conduction in the presence of injection and dissociation–recombination processes plays the key role in major EHD phenomena. The use of multiion conduction models made it possible to explain a vast variety of EHD processes both in the course of their evolution and under steady-state conditions in electrode systems of different geometries and at high-voltage field strengths. For all the apparent paradoxes of electrohydrodynamic phenomena, nonlinear analysis including numerical calculations in the framework of the available models provides an explanation of EHD events based on classical concepts.

Evidently, EHD effects may find application in various technologies, such as the use of EHD flows in fluid pumping (e.g., an EHD pump without moving mechanical parts) or heat exchange enhancement. EHD-based devices may be of use in the aerospace industry due to a number of important advantages (absence of vibrations, noise, etc.). However, the operational life of EHD systems remains too short, which poses problems similar to those encountered in due time in the development of semiconducting materials, like the necessity of high-grade purification of fluids and selection of injection impurities (doping of semiconductors) to maintain reversible redox reactions at the electrodes. We believe it will be possible to resolve these problems in the near future and thereby give a new impetus to the development of electrostatic technologies.

This work was supported by the Federal State Program, 'Academic and Teaching Staff of Innovative Russia', 2009–2013 (state contract P913).

References

1. Melcher J *Magn. Gidrodin.* (2) 3 (1974)
2. Melcher J R, Taylor G I *Annu. Rev. Fluid Mech.* **1** 111 (1969) [Translated into Russian, in *Mekhanika*: *Periodicheskii Sbornik Perevodov Inostrannykh Statei* (Mechanics. Periodic Collection of Translations of Foreign Articles) Issue 5 (Moscow: Mir, 1971) p. 68]
3. Felici N J *Direct Current* (2) 90 (1971)
4. Atten P, Gosse J P *J. Chem. Phys.* **51** 2804 (1969)
5. Felici N, Lacroix J˚ *J. Electrostatics* **5** 135 (1978)
6. Castellanos A *IEEE Trans. Electr. Insul.* **26** 1201 (1991)
7. Mackey A M, Gibbings J C *J. Electrostatics* **10** 257 (1981); Gibbings J C, Mackey A M *J. Electrostatics* **11** 119 (1981)
8. Jones T B *Adv. Heat Transfer* **14** 107 (1979)
9. Gogosov V V, Polyanskii V A, in *Itogi Nauki i Tekhniki. Mekhanika Zhidkosti i Gaza* Vol. 10 (Moscow: VINITI, 1976)
10. Tarapov I E *Teoriya Funktsii, Funktsional'nyi Analiz Ikh Prilozheniya* **17** 221 (1973)
11. Bologa M K, Grosu F P, Kozhukhar' I A *Elektrokonvektsiya i Teploobmen* (Electroconvection and Heat Exchange) (Kishinev: Shtiintsa, 1977)
12. Ostroumov G A *Vzaimodeistvie Elektricheskikh i Gidrodinamicheskikh Polei* (Interaction of Electric and Hydrodynamic Fields) (Moscow: Nauka, 1979)
13. Stishkov Yu K, Ostapenko A A *Elektrogidrodinamicheskie Techeniya v Zhidkikh Dielektrikakh* (Electrohydrodynamic Flows in Liquid Dielectrics) (Leningrad: Izd. LGU, 1989)
14. Gabdukaev G A, Kosvintsev S R, Semenov V A *Izv. Sib. Otd. Akad. Nauk SSSR Ser. Tekh. Nauk* (4) 95 (1990)
15. Berezhnov V V, Semenov V A *Zh. Tekh. Fiz.* **65** (9) 197 (1995) [*Tech. Phys.* **40** 973 (1995)]
16. Semenov V A *Zh. Tekh. Fiz.* **69** (6) 127 (1999) [*Tech. Phys.* **44** 722 (1999)]
17. Skanavi G I *Fizika Dielektrikov*: *Oblast' Slabykh Polei* (Physics of Dielectrics: Weak Field Region) (Moscow: GITTL, 1949)
18. Skanavi G I *Fizika Dielektrikov*: *Oblast' Sil'nykh Polei* (Physics of Dielectrics: Strong Field Region) (Moscow: Fizmatgiz, 1958)
19. Adamczewski I *Jonizacja i Przewodnictwo Cieklych Dielektryków* (Warszawa: Państwowe Wydawn. Naukowe, 1965) [Translated into English: *Ionization, Conductivity and Breakdown in Dielectric Liquids* (London: Taylor & Francis, 1969); Translated into Russian (Leningrad: Energiya, 1972)]
20. Ushakov V Ya *Impul'snyi Elektricheskii Proboi Zhidkostei* (Pulsed Electrical Breakdown in Fluids) (Tomsk: Izd. Tomsk. Univ., 1975)
21. Ushakov V Ya et al. *Proboi Zhidkostei pri Impul'snom Napryazhenii* (Breakdown in Fluids Under Pulsed Voltage) (Tomsk: Izd. Nauch.-Tekh. Lit., 2005)
22. Rubashov I B, Bortnikov Yu S *Elektrogazodinamika* (Electrogasdynamics) (Moscow: Atomizdat, 1971)
23. Castellanos A (Ed.) *Electrohydrodynamics* (CISM Courses and Lectures, No. 380) (Wien: Springer, 1998)
24. Zhakin A I *Usp. Fiz. Nauk* **173** 51 (2003) [*Phys. Usp.* **46** 45 (2003)]
25. Zhakin A I *Usp. Fiz. Nauk* **176** 289 (2006) [*Phys. Usp.* **49** 275 (2006)]
26. Zhakin A I *Electrohydrodynamics*: *Basic Concepts, Problems and Applications* (Kursk: Univ. Press, 1998)
27. Druzhinin É A *Proizvodstvo i Svoistva Fil'truyushchikh Materialov Petryanova iz Ul'tratonkikh Polimernykh Volokon* (Fabrication and Properties of Petryanov's Filter Materials from Ultrathin Filaments) (Moscow: IzdAT, 2007)
28. Alontseva N M et al., in *Sovremennye Problemy Elektrofiziki i Elektrogidrodinamiki Zhidkostei*: *Sb. Dokladov IX Mezhdunar. Nauchn. Konf., 22 Iyunya–26 Iyunya 2009 goda* (Current Problems of Electrophysics and Electrohydrodynamics of Liquids: Proc. of the 9th Intern. Sci. Conf., 22–26 June 2009) (St. Petersburg: Solo, 2009)
29. Vereshchagin I P et al. *Osnovy Elektrogazodinamiki Dispersnykh Sistem* (Fundamentals of Electrogasdynamics of Dispersion Systems) (Moscow: Energiya, 1974)
30. Bezrukov V I *Osnovy Elektrokaplestruinykh Tekhnologii* (Fundamentals of Electrical Droplet and Jet Technologies) (St. Petersburg: Sudostroenie, 2001)
31. Mitskevich P K, Solodovnichenko I M, Sigarev M T *Elektrokhim.* **1** 1072 (1965)
32. Zhakin A I *Magn. Gidrodin.* (4) 41 (1983)
33. Nefedov A P, Petrov O F, Fortov V E *Usp. Fiz. Nauk* **167** 1215 (1997) [*Phys. Usp.* **40** 1163 (1997)]
34. Tamm I E *Osnovy Teorii Elektrichestva* (Fundamentals of the Theory of Electricity) (Moscow: Nauka, 1966) [Translated into English (Moscow: Mir Publ., 1979)]
35. Campbell K H S et al. *Nature* **380** 64 (1996)
36. Smirnov B M *Usp. Fiz. Nauk* **162** (8) 43 (1992) [*Phys. Usp.* **35** 650 (1992)]
37. de Groot S R, Mazur P *Non-equilibrium Thermodynamics* (Amsterdam: North-Holland Publ. Co., 1962) [Translated into Russian (Moscow: Mir, 1964)]
38. Tarapov I E, Zhakin A I, Ievlev I I *Neravnovesnaya Termodinamika i Ee Prilozhenie k Mekhanike Namagnichivayushchikhsya i Polyarizuyushchikhsya Sred* (Non-Equilibrium Thermodynamics and Its Application to Mechanics of Magnetizable and Polarizable Media) (Khar'kov: Khar'kov. Gos. Univ., 1986)
39. Landau L D, Lifshitz E M *Elektrodinamika Sploshnykh Sred* (Electrodynamics of Continuous Media) (Moscow: Nauka, 1982) [Translated into English (Oxford: Pergamon Press, 1984)]
40. Zhakin A I *Fiziko-Khimicheskaya Gidrodinamika Mnogokomponentnykh Dispersnykh Sred* (Physicochemical Hydrodynamics of Multicomponent Dispersed Media) (Kursk: KGTU, 1999)
41. Dobretsov L N, Gomoyunova M V *Emissionnaya Elektronika* (Emission Electronics) (Moscow: Nauka, 1966) [Translated into English (Jerusalem: Israel Program for Sci. Translations, 1971)]
42. Fomenko V S, Podchernyaeva I A *Emissionnye i Adsorbtsionnye Svoistva Veshchestv i Materialov* (Emission and Adsorption Properties of Substances and Materials) (Moscow: Atomizdat, 1975)
43. Gosse B, Gosse J P, Felici N J *J. Appl. Electrochem.* **5** 329 (1975)
44. Izmailov N A *Elektrokhimiya Rastvorov* (Electrochemistry of Solutions) (Moscow: Khimiya, 1966)
45. Zhdanov S I, Gracheva N P, in *Zhidkie Kristally* (Liquid Crystals) (Ed. S I Zhdanov) (Moscow: Khimiya, 1979)
46. Voinov M, Dunnett J S *J. Electrochem. Soc.* **120** 922 (1973)
47. Wolkenstein T *Elektronnye Protsessy na Poverkhnosti Poluprovodnikov pri Khemosorbtsii* (Electronic Processes on Semiconductor Surfaces During Chemisorption) (Moscow: Nauka, 1987) [Translated into English (New York: Consultants Bureau, 1991)]
48. Kiselev V F, Kozlov S N, Zateev A V *Osnovy Fiziki Poverkhnosti Tverdogo Tela* (Fundamentals of Solid Surface Physics) (Moscow: Izd. Mosk. Univ., Fiz. Fak. MGU, 1999)
49. Maissel L I, Glang R *Handbook of Thin Film Technology* (New York: McGraw-Hill, 1970) [Translated into Russian (Moscow: Sov. Radio, 1977)]
50. Partenskii M B *Usp. Fiz. Nauk* **128** 69 (1979) [*Sov. Phys. Usp.* **22** 330 (1979)]
51. Komnik Yu F *Fizika Metallicheskikh Plenok*: *Razmernye i Strukturnye Effekty* (Physics of Metallic Films: Dimensional and Structural Effects) (Moscow: Atomizdat, 1979)
52. Morrison S R *The Chemical Physics of Surfaces* (New York: Plenum Press, 1977) [Translated into Russian (Moscow: Mir, 1980)]

53. Zhakin A I *Izv. Akad. Nauk SSSR Mekh. Zhidk. Gaza* (4) 3 (1986) [*Fluid Dyn.* **21** 507 (1986)]
54. Mesyats G A *Usp. Fiz. Nauk* **165** 601 (1995) [*Phys. Usp.* **38** 567 (1995)]
55. Felici N, Gosse J P *Rev. Phys. Appl.* **14** 629 (1979)
56. Kuz'ko A E, Zhakin A I, in *Neobratimye Protsessy v Prirode i Tekhnike*: *Trudy 6-i Vseross. Konf. 26–28 Yanvarya, 2011 g., Moskva* (Irreversible Processes in Nature and Technology: Proc. of the 6th All-Russian Conf., 26 – 28 January 2011, Moscow) (Moscow: MGTU im. N É Baumana, 2011) p. 271
57. Dikanskii Yu I et al. *Kolloidn. Zh.* **67** 161 (2005) [*Colloid J.* **67** 134 (2005)]
58. Kozhevnikov V M et al. *Zh. Tekh. Fiz.* **78** (2) 51 (2008) [*Tech. Phys.* **53** 192 (2008)]
59. Vasil'ev V A, Romanovskii Yu M, Yakhno V G *Avtovolnovye Protsessy* (Autowave Processes) (M.: Nauka, 1987)
60. Zhakin A I *Vestn. Khar'kov. Gos. Univ. Mekh. Upravlenie Dinam. Sist.* (241) 3 (1983)
61. Saranin V A *Ustoichivost' Ravnovesiya, Zaryadka, Konvektsiya i Vzaimodeistvie Zhidkikh Mass v Elektricheskikh Polyakh* (Stability of Equilibrium, Charging, Convection and Interaction of Liquid Masses in Electric Fields) (Moscow–Izhevsk: RKhD, 2009)
62. Sedov L I *Mekhanika Sploshnoi Sredy* (A Course in Continuum Mechanics) Vol. 1 (Moscow: Nauka, 1973) [Translated into English (Groningen: Wolters-Noordhoff, 1971)]
63. McConnell A J *Application of Tensor Analysis* (New York: Dover Publ., 1957) [Translated into Russian (Moscow: Fizmatgiz, 1963)]
64. Zhakin A I *Tenzornyi Analiz. Mekhanika. Gravitatsiya* (Tensor Analysis. Mechanics. Gravity) (Kursk: KGTU, 1998)
65. Babskii V G et al. *Gidromekhanika Nevesomosti* (Hydromechanics of Weightlessness) (Ed. A D Myshkis) (Moscow: Nauka, 1976)
66. Adamson A W *Physical Chemistry of Surfaces* (New York: Wiley, 1976) [Translated into Russian (Moscow: Mir, 1979)]
67. Ono S, Kondo S *Molecular Theory of Surface Tension in Liquids* (Handbuch der Physik, Ed. S Flügge, Vol. 10) (Berlin: Springer-Verlag, 1960) [Translated into Russian (Moscow: IL, 1963)]
68. Rowlinson J S, Widom B *Molecular Theory of Capillarity* (Oxford: Clarendon Press, 1982) [Translated into Russian (Moscow: Mir, 1986)]
69. Landau L D, Lifshitz E M *Statisticheskaya Fizika* (Statistical Physics) Vol. 1 (Moscow: Nauka, 1976) [Translated into English (Oxford: Pergamon Press, 1980)]
70. Zhakin A I *Elektron. Obrabotka Mater.* (4) 39 (1989)
71. Kosvintsev S R, Thesis for Cand. Phys.-Math. Sci. (Perm': Perm. Gos. Univ., 1993)
72. Castellanos A, Atten P, Velarde M G *Phys. Fluids* **27** 1607 (1984)
73. Rychkov Yu M, Stishkov Yu K *Kolloid. Zh.* **41** 1204 (1978)
74. Thomson J J, Thomson G P *Conduction of Electricity through Gases* Vol. 1, 3rd ed. (Cambridge: Univ. Press, 1928) p. 193
75. Semenikhin N M, Zholkovskii É K *Elektrokhim.* **18** 691 (1982)
76. Zhakin A I *Elektron. Obrabotka Mater.* (2) 48 (1988)
77. Turnbull R J, Melcher J R *Phys. Fluids* **12** 1160 (1969)
78. Turnbull R J *Phys. Fluids* **11** 2597 (1968)
79. Roberts P H *Quart. J. Mech. Appl. Math.* **22** 211 (1969)
80. Zhakin A I *Magn. Gidrodin.* (2) 70 (1982)
81. Zhakin A I, Fedonenko A I *Elektron. Obrabotka Mater.* (4) 41 (1983)
82. Zhakin A I, Tarapov I E, Fedonenko A I *Elektron. Obrabotka Mater.* (5) 37 (1983)
83. Kazatskaya L S, Solodovnichenko I M *Elektron. Obrabotka Mater.* (2) 68 (1979)
84. Stishkov Yu K, Ostapenko A A *Magn. Gidrodin.* (3) 139 (1980)
85. Pohl H A *J. Appl. Phys.* **29** 1182 (1958)
86. Yavorskaya I M, Fomina N I, Belyaev Yu N *Acta Astronautica* **11** 179 (1984)
87. Bogoliubov N N, Mitropolsky Y A *Asimptoticheskie Methody v Teorii Nelineinykh Kolebanii* (Asymptotic Methods in the Theory of Non-linear Oscillations) (Moscow: Nauka, 1974) [Translated into English (New York: Gordon and Breach, 1961)]
88. Gershuni G Z, Zhukhovitskii E M *Konvektivnaya Ustoichivost' Neszhimaemoi Zhidkosti* (Convective Stability of Incompressible Liquid) (Moscow: Nauka, 1972)
89. Vargaftik N B *Spravochnik po Teplofizicheskim Svoistvam Gazov i Zhidkostei* (Tables on the Thermophysical Properties of Liquids and Gases) (Moscow: Nauka, 1972) [Translated into English (Washington: Hemisphere Pub. Corp., 1975)]
90. Gallagher T J *Simple Dielectric Liquids*: *Mobility, Conduction, and Breakdown* (Oxford: Clarendon Press, 1975)
91. Zhakin A I *Izv. Akad. Nauk SSSR Mekh. Zhidk. Gaza* (1) 98 (1983) [*Fluid Dyn.* **18** 78 (1983)]
92. Fedonenko A I, Zhakin A I *Magn. Gidrodin.* (3) 74 (1982)
93. Caldin E *Fast Reactions in Solution* (New York: Wiley, 1964) [Translated into Russian (Moscow: Mir, 1966)]
94. Debye P *J. Chem. Phys.* **1** 13 (1933)
95. Enderby J A *Proc. R. Soc. London A* **207** 329 (1951)
96. Zhakin A I *Izv. Akad. Nauk SSSR Mekh. Zhidk. Gaza* (1) 34 (1989) [*Fluid Dyn.* **24** 27 (1989)]
97. Zhakin A I, Tarapov I E, Fedonenko A I *Magn. Gidrodin.* (4) 139 (1981)
98. Zhakin A I *Vestn. Khar'kovskogo Univ. Matem., Mekh. Voprosy Upravleniya* (298) 7 (1987)
99. Zhakin A I *Izv. Akad. Nauk SSSR Mekh. Zhidk. Gaza* (2) 14 (1988) [*Fluid Dyn.* **23** 168 (1988)]
100. Gosman A D et al. *Heat and Mass Transfer in Recirculating Flows* (London: Academic Press, 1969) [Translated into Russian (Moscow: Mir, 1972)]
101. Bologa M K, Kozhevnikov I V, Mardarskii O I *Elektron. Obrabotka Mater.* (1) 17 (2009) [*Surf. Eng. Appl. Electrochem.* **45** 13 (2009)]